Wigner crystal physics in quantum wires

2009 J. Phys.: Condens. Matter 21 023203

(http://iopscience.iop.org/0953-8984/21/2/023203)

J. Phys.: Condens. Matter **21** (2009) 023203 (20pp) doi:10.1088/0953-8984/21/2/023203

TOPICAL REVIEW

Wigner crystal physics in quantum wires

Julia S Meyer[1] **and K A Matveev**[2]

[1] Department of Physics, The Ohio State University, Columbus, OH 43210, USA
[2] Materials Science Division, Argonne National Laboratory, Argonne, IL 60439, USA

E-mail: jmeyer@mps.ohio-state.edu

Received 29 August 2008, in final form 10 November 2008
Published 10 December 2008
Online at stacks.iop.org/JPhysCM/21/023203

Abstract
The physics of interacting quantum wires has attracted a lot of attention recently. When the density of electrons in the wire is very low, the strong repulsion between electrons leads to the formation of a Wigner crystal. We review the rich spin and orbital properties of the Wigner crystal, in both the one-dimensional and the quasi-one-dimensional regimes. In the one-dimensional Wigner crystal the electron spins form an antiferromagnetic Heisenberg chain with exponentially small exchange coupling. In the presence of leads, the resulting inhomogeneity of the electron density causes a violation of spin–charge separation. As a consequence the spin degrees of freedom affect the conductance of the wire. Upon increasing the electron density, the Wigner crystal starts deviating from the strictly one-dimensional geometry, forming a zigzag structure instead. Spin interactions in this regime are dominated by ring exchanges, and the phase diagram of the resulting zigzag spin chain has a number of unpolarized phases as well as regions of complete and partial spin polarization. Finally we address the orbital properties in the vicinity of the transition from a one-dimensional to a quasi-one-dimensional state. Due to the locking between chains in the zigzag Wigner crystal, only one gapless mode exists. Manifestations of Wigner crystal physics at weak interactions are explored by studying the fate of the additional gapped low-energy mode as a function of interaction strength.

(Some figures in this article are in colour only in the electronic version)

Contents

1. Introduction

First experiments [1, 2] on electronic transport in one-dimensional conductors revealed the remarkable quantization of conductance in multiples of the universal quantum $2e^2/h$, where e is the elementary charge and h is Planck's constant. These experiments were performed by confining two-dimensional electrons in GaAs heterostructures to one dimension by applying a negative voltage to two gates, thereby forcing the electrons to flow from one side of the sample to the other via a very narrow channel. Such devices, typically

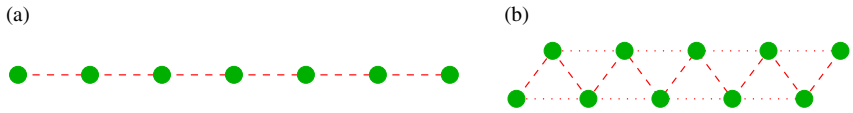

Figure 1. (a) A one-dimensional Wigner crystal formed in a quantum wire at low electron density. (b) The zigzag Wigner crystal forms in a certain regime of densities when the electrons are confined to the wire by a shallow potential.

referred to as quantum point contacts, are the simplest physical realization of a one-dimensional electron system. Although the length of the one-dimensional region in quantum point contacts is relatively short, the quantization of conductance indicates that transport in such devices is essentially one-dimensional. Longer quantum wires have been created later using either a different gate geometry [3], or by confining two-dimensional electrons by other means, such as in cleaved-edge-overgrowth devices [4]. Finally, a fundamentally different way of confining electrons to one dimension has been recently realized in carbon nanotubes [5, 6]. The interest in the study of one-dimensional conductors is stimulated by the relatively low disorder in these systems and by the ability to control their parameters. For instance, the effective strength of the electron–electron interactions is determined by the electron density, which can be tuned by changing the gate voltage. Thus quantum wire devices represent one of the simplest interacting electron systems in which a detailed study of transport properties can be performed.

Interactions between one-dimensional electrons are of fundamental importance. Unlike in higher-dimensional systems, in one dimension the low-energy properties of interacting electron systems are not described by Fermi liquid theory. Instead, the so-called Tomonaga–Luttinger liquid emerges as the proper description of the system in which, instead of fermionic quasiparticles, the elementary excitations are bosons [7]. Interestingly, the quantization of conductance in quantum point contacts is well understood in the framework of noninteracting electrons [8] despite the relatively strong interactions in these devices. This paradox was resolved theoretically [9–11] by considering a Luttinger liquid with position-dependent parameters chosen in a way that models strongly interacting electrons in the quantum wire connected to leads in which interactions can be neglected. It was found that the dc conductance of such a system is completely controlled by the leads, and is therefore insensitive to the interactions.

The latter conclusion is in apparent disagreement with experiments observing the so-called *0.7 structure* in the conductance of quantum point contacts [12–20]. This feature appears as a quasi-plateau of conductance at about $0.7 \times 2e^2/h$ at very low electron density in the wire, and usually grows with temperature. A number of possible explanations have been proposed, most of which attribute the feature to the fact that at low densities the effective interaction strength is strongly enhanced. One of the most common explanations attributes the 0.7 structure to spontaneous polarization of electron spins in the wire [12–18, 20–25]. Although such polarization is forbidden in one dimension [26], the electrons in quantum wires are, of course, three-dimensional, albeit confined to a channel of small width. This deviation from true one-dimensionality may, in principle, give rise to a spin-polarized ground state of the interacting electron system.

The electrons in quantum wires interact via repulsive Coulomb forces. As a result of the long-range nature of the repulsion, at low density the kinetic energy of the electrons is small compared to the interactions. To minimize their repulsion, electrons form a periodic structure called the Wigner crystal [27]. In one dimension the long-range order in the Wigner crystal (figure 1(a)) is smeared by quantum fluctuations [28], and therefore the crystalline state can be viewed as the strongly interacting regime of the Luttinger liquid. However, the presence of strong short-range order provides a clear physical picture of the strongly interacting one-dimensional system and enables one to develop a theoretical description of quantum wires in the low-density regime.

In the Wigner crystal regime the electrons are strongly confined to the vicinity of the lattice sites. As a result the exchange of electron spins is strongly suppressed, and only the nearest-neighbor spins are coupled to each other. One can then think of the electron spins forming a Heisenberg spin chain with a coupling constant J much smaller than the Fermi energy E_F. The presence of two very different energy scales E_F and J for the charge and spin excitations distinguishes the strongly interacting Wigner crystal regime from a generic one-dimensional electron system with moderately strong interactions. In particular, the Luttinger liquid theory is applicable to the Wigner crystal only at the lowest energies, $\varepsilon \ll J$. On the other hand, if any of the important energy scales of the problem exceed J, the spin excitations can no longer be treated as bosons, and the conventional Tomonaga–Luttinger picture fails. One of the most interesting examples of such behavior occurs when the temperature T is in the range $J \ll T \ll E_F$. In this case the charge excitations retain their bosonic properties consistent with Luttinger liquid theory, whereas the correlations of electron spins are completely destroyed by thermal fluctuations. Such one-dimensional systems are not limited to the Wigner crystal regime and are generically referred to as spin-incoherent Luttinger liquids. We argue in section 2 that the coupling of spin and charge excitations in this regime leads to a reduction of the conductance of the quantum wire from $2e^2/h$ to e^2/h. A number of additional interesting properties of spin-incoherent Luttinger liquids are discussed in a recent review [29].

The electrons in a quantum wire are confined to one dimension by an external potential. In the common case of the potential created by negatively charged gates placed on top of a two-dimensional electron system, the confining potential can be rather shallow. In this case the strong repulsion

between electrons can force them to move away from the center of the wire, transforming the one-dimensional Wigner crystal to a quasi-one-dimensional zigzag structure, figure 1(b). In the case of classical electrons such a transition has been studied in [30–32]; we review this theory in section 3. The zigzag Wigner crystal has rich spin properties due to the fact that each electron can now be surrounded by four neighbors with significant spin coupling. Ring exchange processes play an important role and may under certain circumstances give rise to a spontaneous polarization of electron spins. The spin properties of the zigzag Wigner crystals are discussed in section 4.

The transformation of a one-dimensional Wigner crystal to the zigzag shape is a special case of a transition from a one-dimensional to a quasi-one-dimensional state of electrons in a quantum wire. Another such transition occurs in the case of noninteracting electrons when the density is increased until population of the second subband of electronic states in the confining potential begins. These two transitions seem to have rather different properties. Indeed, in the case of noninteracting electrons the population of the second subband entails the emergence of a second acoustic excitation branch in the system. On the other hand, even though the zigzag crystal has two rows, their relative motion is locked, and one expects to find only one acoustic branch in this case. It is therefore interesting to explore how the number of acoustic excitation branches changes as the interaction strength is tuned. In the regime of strong interactions this requires developing the quantum theory of the transition from a one-dimensional to a zigzag Wigner crystal. We discuss such a theory in section 5, where it is shown that quantum fluctuations do not lead to the emergence of a second acoustic branch in the zigzag crystal. This feature of the Wigner crystal survives even at weak interactions, with the second acoustic branch appearing only when the interactions are completely turned off.

2. One-dimensional crystal

2.1. Quantum wire at low electron density

Electrons in a quantum wire repel each other with Coulomb forces. To characterize the strength of interactions, let us compare the typical kinetic energy of an electron, which is of the order of the Fermi energy $E_F \sim \hbar^2 n^2/m$, with the typical interaction energy $e^2 n/\epsilon$. (Here n is the electron density, m is the effective mass, and ϵ is the dielectric constant of the medium.) Clearly, the Coulomb repulsion dominates over the kinetic energy in the low-density regime $na_B \ll 1$, where $a_B = \hbar^2\epsilon/me^2$ is the Bohr's radius in the material. Then the ground state of the system is achieved by placing electrons at well-defined points in the wire, separated from each other by the distance n^{-1}, figure 1(a), thus creating a Wigner crystal. Because the kinetic energy of electrons is small, the amplitude δx of the zero-point fluctuations of electrons near the sites of the Wigner lattice is much smaller than the period of the crystal, $n\delta x \sim (na_B)^{1/4} \ll 1$.

In experiment the quantum wire is usually surrounded by metal gates. As a result, the Coulomb interactions between electrons are screened at large distances by image charges in the gates. For example, if the gate is modeled by a metal plane at distance d from the wire, the interaction potential becomes

$$V(x) = \frac{e^2}{\epsilon}\left(\frac{1}{|x|} - \frac{1}{\sqrt{x^2+(2d)^2}}\right). \tag{1}$$

At large distances this potential falls off as $V(x) \sim 2e^2d^2/\epsilon|x|^3$, much more rapidly than the original Coulomb repulsion. As a result, in the limit $n \to 0$ the crystalline ordering of electrons will be destroyed by quantum fluctuations. Comparison of the Fermi energy with the screened Coulomb repulsion (1) shows that the Wigner crystal exists in the range of densities $a_B d^{-2} \ll n \ll a_B^{-1}$, provided that the distance to the gate $d \gg a_B$. In typical experiments with GaAs quantum wire devices $a_B = 10$ and $d \gtrsim 100$ nm; thus the Wigner crystal state should persist until unrealistically low densities $\sim 10^{-3}$ nm^{-1}.

Similar to phonons in conventional crystals, the Wigner crystal supports acoustic plasmon excitations—propagating waves of electron density. The speed of plasmons is given by[3]

$$s = \sqrt{\frac{2e^2 n}{\epsilon m}\ln(8.0nd)}. \tag{2}$$

The Hamiltonian describing these low-energy excitations is easily obtained by treating the Wigner crystal as a continuous medium. Adding the kinetic energy and the potential energy of elastic deformation, one obtains

$$H_\rho = \int \left[\frac{p^2}{2mn} + \frac{1}{2}mns^2(\partial_x u)^2\right] \mathrm{d}x, \tag{3}$$

where $u(x)$ is the displacement of the medium at point x from its equilibrium position, and $p(x)$ is the momentum density. In one dimension the acoustic excitations destroy the long-range order in the crystal even at zero temperature, $\langle[u(x)-u(0)]^2\rangle \simeq (\hbar/\pi mns)\ln nx$.[4]

In the model of spinless electrons, Hamiltonian (3) accounts for all possible low-energy excitations of the system. However, in the presence of spins, there are additional excitations not included in (3). In the Wigner crystal regime the electrons are localized near their lattice sites, figure 1(a), and to a first approximation the spins at different sites are not coupled. The exchange coupling of two spins at neighboring sites occurs via the process of two electrons switching their places on the Wigner lattice. When the electrons approach each other, the strong Coulomb repulsion creates a high potential barrier. As a result, the exchange processes are very weak, and only the coupling of the nearest-neighbor spins needs to be taken into account. The Hamiltonian describing the spin excitations takes the form

$$H_\sigma = \sum_l J\, \boldsymbol{S}_l \cdot \boldsymbol{S}_{l+1}, \tag{4}$$

[3] The result (2) was derived in [33] for densities in the range $d^{-1} \ll n \ll a_B^{-1}$. Extending their calculation to the density range $a_B/d^2 \ll n \ll d^{-1}$, one finds $s = [24e^2n^3d^2\zeta(3)/\epsilon m]^{1/2}$.

[4] In the absence of the screening gate the plasmon speed s diverges at small wavevectors, see (2) at $d \to \infty$. Although this effect suppresses the quantum fluctuations, it is not sufficient to restore the long-range order [28].

where $\boldsymbol{S}_l$ is the spin at site l. As the exchange processes involve tunneling through a high barrier, the exchange constant is exponentially suppressed [34–36],

$$J \propto \exp\left(-\frac{\eta}{\sqrt{n a_{\mathrm{B}}}}\right), \tag{5}$$

where $\eta \approx 2.80$ [50–52], see also section 4.1.1. Taken together, equations (3) and (4) account for all low-energy excitations of the one-dimensional Wigner crystal, i.e., the Hamiltonian of the system can be represented as the sum

$$H = H_\rho + H_\sigma. \tag{6}$$

Because of the absence of long-range order, one expects that in the low-energy limit the Wigner crystal should be a special case of the Luttinger liquid. The latter is commonly described [7] by a Hamiltonian of the form (6), with the charge and spin Hamiltonians, H_ρ and H_σ, given by

$$H_\rho = \int \frac{\hbar u_\rho}{2\pi}\left[\pi^2 K_\rho \Pi_\rho^2 + K_\rho^{-1}(\partial_x \phi_\rho)^2\right] \mathrm{d}x, \tag{7}$$

$$H_\sigma = \int \frac{\hbar u_\sigma}{2\pi}\left[\pi^2 K_\sigma \Pi_\sigma^2 + K_\sigma^{-1}(\partial_x \phi_\sigma)^2\right] \mathrm{d}x + \frac{2 g_{1\perp}}{(2\pi\alpha)^2}\int \cos\left[\sqrt{8}\phi_\sigma(x)\right] \mathrm{d}x. \tag{8}$$

Here the bosonic fields $\phi_{\rho,\sigma}$ and $\Pi_{\rho,\sigma}$ describe the charge (ρ) and spin (σ) excitations propagating with velocities $u_{\rho,\sigma}$. They obey canonical commutation relations $[\phi_\alpha(x), \Pi_{\alpha'}(y)] = \mathrm{i}\delta_{\alpha\alpha'}\delta(x-y)$. In the case of repulsive interactions, the Luttinger liquid parameter K_ρ is in the range $0 < K_\rho < 1$. The cosine term in (8) is marginally irrelevant, i.e., the coupling constant $g_{1\perp}$ scales to zero logarithmically at low energies. At the same time, the parameter K_σ approaches unity as $K_\sigma = 1 + g_{1\perp}/2\pi u_\sigma$.

Both Hamiltonians (3) and (7) describe propagation of elastic waves in the medium. Their formal equivalence is established [36] by identifying

$$\phi_\rho(x) = \frac{\pi n}{\sqrt{2}}u(x), \qquad \Pi_\rho(x) = \frac{\sqrt{2}}{\pi n \hbar}p(x), \qquad u_\rho = s, \qquad K_\rho = \frac{\pi\hbar n}{2ms}. \tag{9}$$

On the other hand, even though both Hamiltonians (4) and (8) describe spin excitations in the system, their equivalence is not obvious. Indeed, Hamiltonian (4) is expressed in terms of spin operators $\boldsymbol{S}_l$ of the electrons, whereas its Luttinger liquid analog (8) is expressed in terms of the bosonic fields ϕ_σ and Π_σ. The connection is established via the well-known procedure [7] of bosonization of the Heisenberg spin chain (4). This procedure is applicable at energies much smaller than the exchange constant J, and reduces Hamiltonian (4) to the form (8), see [36]. One therefore concludes that at low energies the Wigner crystal can indeed be viewed as a Luttinger liquid.

It is important to point out, however, that the equivalence of the Wigner crystal and Luttinger liquid holds only at very low energies, $\varepsilon \ll J$. Given the exponential dependence (5) of the exchange constant on density, one can easily achieve a regime when an important energy scale, such as the temperature, is larger than J. In this case the bosonization procedure leading to (8) is inapplicable, and the form (4) should be used instead. On the other hand, as long as temperature and other relevant energy scales are smaller than the Fermi energy, the charge excitations are bosonic and adequately described by either Hamiltonian (3) or (7).

2.2. Spin–charge separation in the one-dimensional Wigner crystal

The Hamiltonian (6)–(8) of the Luttinger liquid consists of two separate commuting contributions associated with the charge and spin degrees of freedom. Consequently, the low-energy excitations of the system are charge and spin waves, decoupled from each other, and propagating at different velocities u_ρ and u_σ. The operator annihilating a (right-moving) electron with spin γ in this theory has the form

$$\psi_{\mathrm{R}\gamma}(x) = \frac{\mathrm{e}^{\mathrm{i}k_{\mathrm{F}}x}}{\sqrt{2\pi\alpha}}\exp\left\{\frac{\mathrm{i}}{\sqrt{2}}[\phi_\rho(x) - \theta_\rho(x)]\right\} \times \exp\left\{\pm\frac{\mathrm{i}}{\sqrt{2}}[\phi_\sigma(x) - \theta_\sigma(x)]\right\}, \tag{10}$$

in which the charge and spin contributions explicitly factorize. (Here α is a short-distance cutoff, $k_{\mathrm{F}} = \pi n/2$ is the Fermi wavevector of the electrons, and the $\pm$ sign corresponds to electron spin $\gamma = \uparrow, \downarrow$.)

The Hamiltonian of the Wigner crystal (6) also consists of two commuting contributions describing the charge and spin degrees of freedom, with the main difference being the different form (4) of H_σ. However, the analogy with the Luttinger liquid is not complete, as the electron annihilation operator no longer factorizes [37, 38],

$$\psi_{\mathrm{R}\gamma}(x) = \frac{\mathrm{e}^{\mathrm{i}2k_{\mathrm{F}}x}}{\sqrt{2\pi\alpha}} \times \exp\left\{\frac{\mathrm{i}}{\sqrt{2}}[2\phi_\rho(x) - \theta_\rho(x)]\right\} Z_{l,\gamma}\Big|_{l = nx + \frac{\sqrt{2}}{\pi}\phi_\rho(x)}. \tag{11}$$

Here the operator $Z_{l,\gamma}$ acts upon any state of the spin chain (4) and produces a state with one less spin by removing spin γ at site number l. The form of the fermion operator (11) reflects the fact that when an electron is removed from the Wigner crystal, one of the sites of the spin chain (4) is also removed. In the absence of plasmon excitations, the sites are equidistant, and the site at point x has the number $l = nx$. On the other hand, if plasmons propagate though the crystal, the electrons shift by a distance proportional to ϕ_ρ, and the spin is removed from the site $l = nx + \frac{\sqrt{2}}{\pi}\phi_\rho(x)$, see (11). Thus the absence of factorization of the charge and spin components of the fermion operator (11) reflects the simple fact that the spins $\boldsymbol{S}_l$ in the spin chain (4) are attached to the electrons.

The absence of spin–charge separation in the Hamiltonian of the Wigner crystal manifests itself if the system is not uniform, such as in the case of a quantum wire with a low electron density that depends on position, $n = n(x)$. Assuming that the variations of $n(x)$ occur at a length scale much larger than the distance between electrons, one can still bosonize the charge modes near every point in space, while accounting for

the x-dependence of the parameters u_ρ and K_ρ. Thus one obtains

$$H_\rho = \int \frac{\hbar u_\rho(x)}{2\pi} \left\{\pi^2 K_\rho(x)\Pi_\rho^2 + [K_\rho(x)]^{-1}(\partial_x\phi_\rho)^2\right\} \mathrm{d}x. \tag{12}$$

The exchange constant J in the Hamiltonian (4) of the spin chain also acquires an x-dependence, as it clearly depends on the electron density, see (5). Thus the spin Hamiltonian takes the form

$$H_\sigma = \sum_l J\left[l - \frac{\sqrt{2}}{\pi}\phi_\rho(x_l)\right] \boldsymbol{S}_l \cdot \boldsymbol{S}_{l+1}, \tag{13}$$

where x_l is the initial position of the lth electron. The appearance of the charge field ϕ_ρ in H_σ again accounts for the fact that the plasmons shift the site l of the spin chain from its initial position by $\frac{\sqrt{2}}{\pi}\phi_\rho$. Therefore the two contributions H_ρ and H_σ to the Hamiltonian of the Wigner crystal commute only in the uniform system, when the exchange constant J does not depend on position.

2.3. Conductance of a Wigner crystal wire

In experiment, the quantum wires are usually made by confining a two-dimensional electron system to a one-dimensional channel. One of the most common techniques is to place two metal electrodes above a GaAs heterostructure in which a two-dimensional electron system is formed, figure 2. When a negative voltage is applied to the gates, the resulting electrostatic potential repels the electrons from the regions covered by the gates, but a narrow channel of electrons between the gates may still remain. The resulting quantum wire connects two large regions of two-dimensional electrons, which play the role of contacts to the wire. If the gate voltage V_g is properly tuned, the electron density in the center of the wire can be sufficiently low for a Wigner crystal to form. On the other hand, the gates do not affect the electron density and the nature of the electron liquid in the two-dimensional leads.

The physics of interacting electrons in two or three dimensions is very different from that of one-dimensional systems. Although at extremely low densities the electrons will form a Wigner crystal, this does not happen in typical GaAs heterostructures. Instead, the electrons are believed to be in a conventional Fermi liquid state with quasiparticle excitations obeying Fermi statistics and carrying the charge of a single electron. In a one-dimensional system such a situation may only occur in the absence of interactions, as otherwise a Luttinger liquid state with bosonic excitations is formed. In the absence of interactions, however, the Fermi liquid and Luttinger liquid pictures are equivalent. Thus it is convenient to model the quantum wire device by a one-dimensional model with position-dependent interactions and electron density. In the central part of the system the density is small so that the interactions may be effectively strong. This region models the quantum wire. As one moves away from the central region, the density grows, the interactions become small, and asymptotically at large distances the electrons become noninteracting. These two semi-infinite noninteracting regions model the two-dimensional leads.

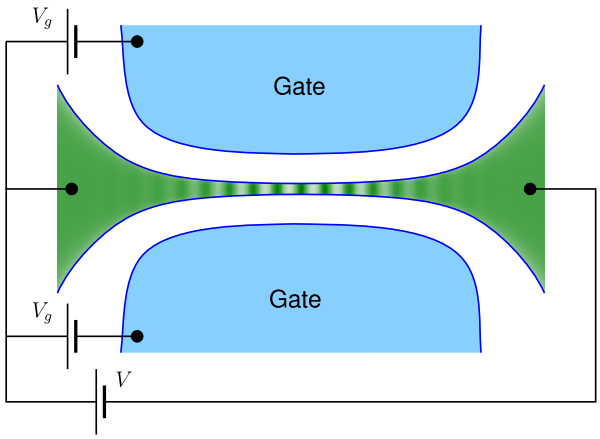

Figure 2. A quantum wire formed by applying negative voltage to the gates placed on top of a two-dimensional electron system. Electrons in the narrow channel between the gates are one-dimensional and their density is sufficiently low to achieve the Wigner crystal regime. Away from the center of the wire the electron density increases, and even the short-range ordering of electrons is destroyed by quantum fluctuations.

Such a model was used in [9–11] to calculate the conductance of a quantum wire described by the Luttinger liquid model. The Hamiltonian studied was essentially identical to (12), as the electrons were assumed to be spinless and only charge modes needed to be accounted for. It was demonstrated that the dc conductance of the wire is not affected by the interactions and remains quantized at e^2/h. Let us illustrate this result with a simple semiclassical calculation.

We start with the homogeneous wire, and for simplicity, instead of the Hamiltonian (7) we will use the equivalent form (3). Unlike papers [9–11], where a term was added to the Hamiltonian in order to describe the bias voltage applied to the wire at point $x = 0$, we consider a setup in which the wire is connected to a current source. A small ac current with frequency ω can be represented in terms of the velocity $\dot{u}$ of the elastic medium and the electron density as

$$ne\dot{u}|_{x=0} = I_0 \cos\omega t. \tag{14}$$

This expression should be viewed as a time-dependent boundary condition imposed on the elastic medium. As a result the medium begins to move periodically with frequency ω, and plasmons propagating into the infinite leads dissipate power $W = I_0^2 R/2$ from the current source, where R is the resistance of the system. Let us calculate W in terms of the parameters of the elastic medium. Since the plasmons carry the energy of the oscillating medium in two directions at speed s, we can express the dissipated power as

$$W = 2s\langle\mathcal{E}\rangle, \tag{15}$$

where $\langle\mathcal{E}\rangle$ is the energy density of the system. The latter consists of two contributions, the kinetic and potential energies represented by the two terms in (3). In a harmonic system the time-averaged values of the kinetic and potential energies are equal, so we will evaluate $\langle\mathcal{E}\rangle$ by doubling the kinetic energy,

$$\langle\mathcal{E}\rangle = mn\dot{u}^2 = \frac{m}{e^2 n} I_0^2 \langle\cos^2\omega t\rangle = \frac{m}{2e^2 n} I_0^2, \tag{16}$$

where we expressed the velocity $\dot{u}$ in terms of the current using (14). Substituting this expression into (15) and comparing the result with the Joule heat law $W = I_0^2 R/2$, we find the resistance

$$R = \frac{2ms}{e^2 n} = \frac{h}{e^2}\frac{s}{v_F}, \tag{17}$$

where we used the density $n = k_F/\pi$ for spinless electrons and defined the Fermi velocity in the interacting system as $v_F = \hbar k_F/m$.

In the noninteracting limit, where the Luttinger liquid theory reproduces the low-energy properties of the Fermi gas, the plasmon velocity $s = v_F$, and we recover the well-known result $R = h/e^2$. The model considered in [9–11] was described by the Hamiltonian (12) of the inhomogeneous Luttinger liquid, where the interactions are present only in a region of finite size L, modeling the wire, and vanish at $x \to \pm\infty$. It is easy to see that the above calculation of the resistance is applicable to such a system as long as the low-frequency limit is considered. Indeed, at $\omega \to 0$ the wavelength of the plasmons $\sim s/\omega$ is much larger than L, so the emission of the plasmons occurs in the noninteracting leads. Thus we have recovered the result [9–11] for the conductance, $G = e^2/h$.

Our simple calculation also enables us to interpret the absence of corrections to the conductance due to electron–electron interactions in a finite region of a one-dimensional system. In the Luttinger liquid theory the main effect of the interactions is to change the compressibility of the electron system, thereby affecting the second term in (3). In the dc limit the wavelength of the plasmons is infinitely large, and thus the deformation $\partial_x u$ within the finite-size interacting region is negligible. Thus the system behaves as a noninteracting one.

The above result for the spinless Luttinger liquid can be easily generalized to the case of electrons with spin. As we discussed in section 2.2, within the Luttinger liquid approximation the charge and spin degrees of freedom are not coupled. Thus the applied bias or electric current couples only to the charge modes, and the above discussion can be repeated with the only modification being the different relation $n = 2k_F/\pi$ between the density and the Fermi wavevector. Substituting this expression instead of $n = k_F/\pi$ in (17) we find the resistance of the charge modes

$$R_\rho = \frac{h}{2e^2}, \tag{18}$$

and thus the expected doubling of the conductance, $G = 2e^2/h$.

On the other hand, we saw in section 2.2 that in the inhomogeneous Wigner crystal there is no spin–charge separation, i.e., the Hamiltonian (13) of the spin excitations depends explicitly on the charge field ϕ_ρ. One can therefore expect that the spin degrees of freedom will affect conductance when the Wigner crystal is not equivalent to the Luttinger liquid. Indeed, we show below that the spins have a significant effect on the electronic transport at temperatures $T \gtrsim J$.

In treating a one-dimensional Wigner crystal attached to noninteracting leads one has to overcome a fundamental problem caused by the lack of quantitative theory for the crossover regions that connect them, figure 2. In the case of spinless electrons both the Wigner crystal and the leads can be viewed as special cases of the Luttinger liquid, assuming that one is only interested in the low-energy properties of the system. Thus one can use the model (12) of the inhomogeneous Luttinger liquid and obtain reliable results, provided that the exact form of the x-dependences of the parameters is not important. In the presence of spins there is an additional complication caused by the fact that the spin sector of a Wigner crystal is described by the Hamiltonian of a Heisenberg spin chain (4) because the spins are attached to well-localized electrons. Such a description is appropriate in neither the crossover region nor the leads, where the short-range crystalline order is absent. In our further discussion we will nevertheless use the model of the inhomogeneous spin chain (13) for the whole system. This model is justified if the temperature is small compared to the Fermi energy in the center of the wire. When one moves away from the center, the density n grows, and consequently the exchange constant J rapidly grows, see (5). Even if in the center of the system we had $J \ll T$, the crossover regime $J \sim T$ will occur while the wire is still in the Wigner crystal regime, as J is still small compared to E_F. Eventually, when one moves sufficiently far from the center of the wire the exchange J becomes of order E_F, and the spin chain model is no longer appropriate. However, since in those regions we have $J \gg T$, the Heisenberg model (4) is equivalent to the spin sector (8) of the Luttinger liquid theory appropriate for both the crossover regions and the leads. Thus, at $T \ll E_F$, one can describe the spin properties of the system by the model (13) of an inhomogeneous spin chain as long as the exact shape of the dependence $J(l)$ does not affect the results.

Formally the quantum wire will be described by the Hamiltonian $H_\rho + H_\sigma$ given by (12) and (13). The electron density has a minimum at the center of the wire, resulting in an exponentially small exchange constant J, figure 3. Far from the center of the wire the exchange constant reaches the value $J_\infty \sim E_F$. Since J depends on position, the spin excitations are coupled to the charge excitations. To find the resulting correction to the conductance of the wire, it is convenient to consider the setup of fixed current through the wire. Given the standard bosonization relation between $\partial_x \phi_\rho$ and the electron density, by fixing the current I at point $x = 0$ one imposes the boundary condition $\phi_\rho(0, t) = -(\pi/\sqrt{2})q(t)$ on the charge modes, where $q(t)$ is the charge transferred through the wire, i.e., $I = e\dot{q}$. As discussed above, at small frequencies ω the plasmon wavelength is very large, and electrons move in phase over distances much longer that the length of the wire. One can therefore replace $\phi_\rho(x)$ by its value at $x = 0$ everywhere within the range where J depends on position, and convert the Hamiltonian (13) to the form

$$H_\sigma = \sum_l J[l + q(t)]\, \boldsymbol{S}_l \cdot \boldsymbol{S}_{l+1}. \tag{19}$$

The advantage of this form of H_σ is that it now commutes with H_ρ. This does not mean that spin–charge separation is restored, as the spin excitations are still affected by the electric current.

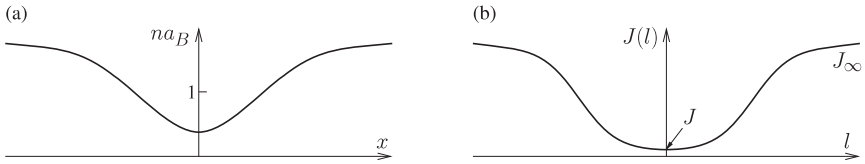

Figure 3. (a) The electron density as a function of position has a minimum in the center of the wire ($x = 0$), where $na_B \ll 1$ and the Wigner crystal is formed. In the lead regions, na_B is assumed to be large such that the interactions can be neglected. (b) The low density in the wire results in the exponential suppression (5) of the exchange constant J. In the lead regions $J(l)$ saturates at $J_\infty \sim E_F$.

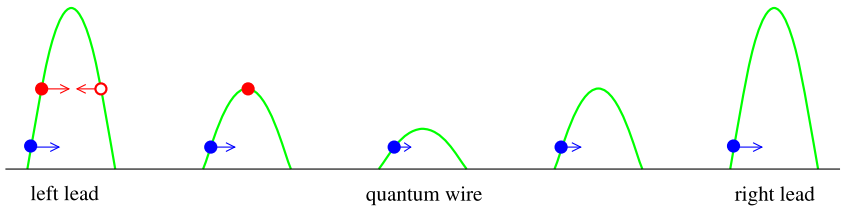

Figure 4. Scattering of spinons at the quantum wire. Spinons with energies below $\pi J/2$ slow down in the wire, but continue to move forward to the opposite lead. Spinons with energies above $\pi J/2$ stop before they reach the center of the wire and are scattered back.

An immediate consequence of the commutativity of H_ρ and H_σ is that the application of electric current through the wire gives rise to independent excitation of the charge and spin modes. Assuming that the power dissipated in each channel is quadratic in current, we conclude $W \equiv I_0^2 R/2 = I_0^2(R_\rho + R_\sigma)/2$. Thus the resistance of the wire is a sum,

$$R = R_\rho + R_\sigma, \tag{20}$$

of two independent contributions due to the charge and spin excitations. Since we have already discussed the contribution (18) of the charge excitations, we now turn our attention to R_σ.

The spin contribution to the resistance depends crucially on whether the temperature is small or large compared to the value J of the exchange constant in the center of the wire, see figure 3. At $T \ll J$ one can bosonize the spin excitations, i.e., convert H_σ to the form (8) with position-dependent parameters. Within this approach, an attempt to account for the coupling to the charge modes in (13) would result in corrections cubic in the bosonic fields. Such corrections are irrelevant perturbations, which are usually neglected as their contribution vanishes at $T \to 0$. Thus one concludes that $R_\sigma = 0$ in the limit $T/J \to 0$.

The absence of dissipation in the spin channel at low temperature can be interpreted as follows. The low-energy excitations of a Heisenberg spin chain are the so-called spinons [39] with spectrum

$$\varepsilon(k) = \frac{\pi J}{2} \sin k, \tag{21}$$

where the wavevector k is defined in the interval $(0, \pi)$. At low temperature the state of the spin chain can be viewed as a dilute gas of spinons. Let us consider propagation of spinons in the spin chain (19) with non-uniform J, figure 3(b), assuming for the moment $q(t) = 0$. If the variation of $J(l)$ is very gradual, one can use the spectrum (21) with l-dependent exchange J. As a spinon propagates through the wire, its energy is conserved, but its momentum and velocity change because of the variation of J along the system. Clearly, if the energy of a spinon is less than $\pi J/2$, where J is the smallest value of the exchange constant in the system, figure 3(b), it passes through the wire without scattering. Conversely, spinons with energies exceeding $\pi J/2$ are backscattered, figure 4.

At $q(t) \neq 0$ the dependence $J(l)$ shown in figure 3(b) is not static, but rather oscillates in position with respect to the spin chain. (More physically, the ac current moves the Wigner crystal with respect to the quantum wire, causing the time dependence of the exchange constants in (19).) The spinons passing through the wire without scattering are not affected by this oscillation. On the other hand, the spinons with energies $\varepsilon > \pi J/2$ are reflected by a *moving* scatterer. Such processes do change the energy of the spinons, and eventually lead to dissipation. At low temperature $T \ll J$ the density of such (thermally-activated) spinons is very low, and one expects only an exponentially small resistance in this regime,

$$R_\sigma \propto \exp\left(-\frac{\pi J}{2T}\right), \qquad T \ll J. \tag{22}$$

It is worth mentioning that the resistance (22) is caused by excitations with energies of the order of the spinon bandwidth J. Such a correction cannot in principle be obtained by the bosonization procedure, which is accurate only at energies much smaller than J.

The expression (22) implies that the resistance R_σ grows with temperature. At $T \gg J$ one expects this growth to saturate. Indeed, in this limit one can assume that $J = 0$ in the center of the wire, i.e., the propagation of spin excitations through the wire is no longer possible. On the other hand, in the leads one still has $T \ll J_\infty \sim E_F$, and the picture of a dilute spinon gas still applies. Every spinon moving toward the wire is reflected back, resulting in a finite dissipation that no longer depends on J.

Unfortunately, one cannot easily develop the theory of scattering of spinons in this regime, as such processes occur in the region where $J(l) \sim T$, and the spinon gas is no longer dilute. One can, however, conjecture that the dissipation resulting from all the spin excitations being reflected by the wire is universal in the sense that it does not depend on the exact nature of the scatterer. Thus if one can solve another problem where all the spin excitations in a one-dimensional system are reflected by a moving scatterer, the result for R_σ should be the same. The simplest example of such a problem is obtained in the same Wigner crystal setup in the presence of a magnetic field B sufficient to polarize electrons in the center of the wire, $T, J \ll \mu_B B \ll E_F$, where μ_B is the Bohr magneton. Then only the electrons with spin directed along the field propagate through the wire whereas the electrons with opposite spin are confined to the leads. This problem can be easily solved in the framework of the bosonization approach [36], resulting in

$$R_\sigma = \frac{h}{2e^2}, \qquad T \gg J. \tag{23}$$

The result is easily understood by noticing that in combination with (20) and (18) one finds the conductance $G = e^2/h$ which is the expected result for the conductance of a spin-polarized wire, where only one type of charge carriers participates in conduction. By our conjecture, the same reduction of conductance from $2e^2/h$ to e^2/h occurs in the absence of the field, provided $J \ll T$, because in both cases all the spin excitations are reflected by the wire, resulting in the same dissipation. This conclusion is consistent with some of the measurements of the conductance of quantum wires a low density [14, 15, 17, 18], showing a small plateau at $G = e^2/h$.

3. Classical transition to the zigzag structure

In section 2, we discussed the physics of a purely one-dimensional crystal. Experimentally, however, quantum wires are created by confining three-dimensional electrons to a narrow channel by an external confining potential. The electron system in the wire can be viewed as one-dimensional as long as the typical energy of the transverse motion is large compared with all other important energy scales; otherwise, deviations from one-dimensionality arise. The remainder of this review addresses the resulting quasi-one-dimensional physics, starting with the classical transition from a one-dimensional to a quasi-one-dimensional Wigner crystal that was studied in [30–32].

To be specific, we consider here a confining potential that mimics the experimental situation. In a typical setup the confining potential in one direction, say the z-direction, is provided by the band bending at the interface of two semiconductors with different band structure (typically GaAs and AlGaAs). This provides a very tight confinement and, correspondingly, the energy scales for transverse excitations are large. Therefore, at low energies, the possibility of electron motion in the z-direction may be neglected. By contrast, confinement in the y-direction is provided by nearby metallic gates which create a relatively shallow confining potential. Deviations from one-dimensionality arise due to lateral displacements in this shallow potential which may be assumed parabolic:

$$V_{\rm conf} = \tfrac{1}{2} m\Omega^2 \sum_i y_i^2, \tag{24}$$

where Ω is the frequency of harmonic oscillations in the confining potential, and y_i is the transverse coordinate of the electron at site i.

As the electron density n grows, so does the typical energy $V_{\rm int} \sim (e^2/\epsilon)n$ of the Coulomb interaction between electrons. Eventually, it becomes energetically favorable for electrons to move away from the axis of the wire. This happens when the distance between particles is of the order of the length scale

$$r_0 = \sqrt[3]{\frac{2e^2}{\epsilon m\Omega^2}}, \tag{25}$$

defined by the condition that the confinement and the Coulomb repulsion, $V_{\rm conf}(r_0) = \frac{1}{2}m\Omega^2 r_0^2$ and $V_{\rm int}(r_0) = e^2/\epsilon r_0$, are equal [32].

The quasi-one-dimensional arrangement that maximizes the distance between electrons—and consequently minimizes the Coulomb interaction energy $V_{\rm int} = (e^2/\epsilon)\sum_{i<j}|\mathbf{r}_i - \mathbf{r}_j|^{-1}$—at a given cost of confining potential energy is a zigzag structure, see figure 1(b). The exact shape of the zigzag crystal can be found by minimizing its energy per particle

$$E = \frac{e^2}{\epsilon r_0}\left\{\frac{\nu}{2}\sum_{l=1}^{\infty}\left(\frac{1}{l} + \frac{1}{\sqrt{(l-\frac{1}{2})^2 + \frac{\nu^2 w^2}{4r_0^2}}}\right) + \frac{w^2}{4r_0^2}\right\} \tag{26}$$

with respect to the distance w between the two rows of the zigzag crystal. Here $\nu = nr_0$ is the dimensionless density, the first two terms account for the interactions between electrons within the same row and in different rows of the zigzag structure, respectively, and the last term stems from the confining potential.

One finds that the distance between rows is given by the solution of the equation

$$\left(\frac{\nu^3}{4}\sum_{l=1}^{\infty}\frac{1}{\left[(l-\frac{1}{2})^2 + \frac{\nu^2 w^2}{4r_0^2}\right]^{3/2}} - 1\right) w = 0. \tag{27}$$

Below the critical density [30, 31]

$$\nu_c = \sqrt[3]{\frac{4}{7\zeta(3)}} \approx 0.780, \tag{28}$$

the only solution is $w = 0$ and, therefore, the crystal is one-dimensional. At densities, $\nu > \nu_c$, a lower-energy solution with $w \neq 0$ appears, and the zigzag structure is formed. The distance between the two rows of the zigzag crystal grows with density. In particular, just above the transition point ν_c, the distance between rows behaves as $w = r_0[\sqrt{24/93\zeta(5)}/\nu_c^2]\sqrt{\delta\nu}$, where $\delta\nu = \nu - \nu_c$. Upon further increasing the density, the zigzag crystal eventually becomes unstable at $\nu \approx 1.75$. At larger densities, $\nu > 1.75$, structures with more than two rows are energetically favorable [32].

Such a classical description of the system is valid only in the limit where the distance between electrons is much larger than the Bohr's radius, $n^{-1} \gg a_B$. As the zigzag regime corresponds to distances between electrons of order r_0, it can only be achieved if r_0 is sufficiently large, $r_0 \gg a_B$. This motivates the introduction of a density-independent parameter

$$r_\Omega = \frac{r_0}{a_B}, \tag{29}$$

which characterizes the strength of Coulomb interactions with respect to the confining potential. If $r_\Omega \ll 1$, as the electron density grows, the interactions become weak at $n \sim a_B^{-1} \ll r_0^{-1}$. As a result, the one-dimensional Wigner crystal melts by quantum fluctuations before the zigzag regime is reached. By contrast, if $r_\Omega \gg 1$, interactions are still strong ($na_B \ll 1$) at densities $n \sim r_0^{-1}$, and the classical description of the transition to the zigzag regime is applicable. As $r_\Omega \propto \Omega^{-2/3}$, the strongly interacting case therefore requires a shallow confining potential. Note that the condition $r_\Omega \gg 1$ can be rewritten as $W \gg a_B$, where $W = \sqrt{\hbar/m\Omega}$ is the (quantum) width of the wire.

4. Spin properties of zigzag Wigner crystals

In a Wigner crystal electrons are localized near their lattice positions due to the mutual Coulomb repulsion. The potential landscape thus created is such that any deviation from these lattice positions incurs an increase in Coulomb energy. In particular, the exchange processes which give rise to spin–spin interactions require tunneling of electrons through the Coulomb barrier that separates them. As pointed out in section 2.1, the resulting spin couplings in a one-dimensional crystal are fairly simple: as the tunneling amplitude decays exponentially with distance, only nearest-neighbor exchange processes have to be taken into account. Thus, the spin degrees of freedom of a one-dimensional Wigner crystal are described by an antiferromagnetic Heisenberg chain (4) with nearest-neighbor exchange energy J whose properties were discussed in section 2.

In a zigzag chain, spin couplings become more interesting. Close to the zigzag transition, the nearest-neighbor exchange is dominant as in the one-dimensional case. However, as the zigzag structure becomes more pronounced each electron is surrounded by four close neighbors rather than only two as in the one-dimensional crystal, and, therefore, the next-nearest neighbor couplings can no longer be neglected. Instead of one coupling constant, one needs to take into account a nearest-neighbor exchange constant J_1 and a next-nearest neighbor exchange constant J_2. Both couplings are antiferromagnetic and, therefore, compete with each other. If J_2 is large enough ($J_2 \gtrsim 0.24\ldots J_1$ [40–42]), the antiferromagnetic ground state gives way to a dimer phase characterized by a non-vanishing order parameter $D \propto \langle (\boldsymbol{S}_{2i+1} - \boldsymbol{S}_{2i-1}) \cdot \boldsymbol{S}_{2i} \rangle$ and a resulting spin gap. The dimer structure is particularly simple on the so-called Majumdar–Ghosh [43, 44] line $J_2 = 0.5J_1$, where the dimers are just nearest-neighbor singlets. The magnitude of the spin gap is a non-monotonic function of the ratio J_2/J_1: it reaches its maximum close to the Majumdar–Ghosh line and becomes exponentially small at $J_2 \gg J_1$.

It turns out, however, that these two-particle exchanges are not sufficient to describe the spin physics of the zigzag crystal. In addition, ring exchanges, i.e., cyclic exchanges of $n \geqslant 3$ particles, have to be taken into account. Defining exchange constants in such a way that they are all positive, the Hamiltonian of the system then reads

$$H_{\text{ring}} = \tfrac{1}{2} \sum_l (J_1 P_{l\,l+1} + J_2 P_{l\,l+2} - J_3 (P_{l\,l+1\,l+2} + P_{l+2\,l+1\,l}) + J_4 (P_{l\,l+1\,l+3\,l+2} + P_{l+2\,l+3\,l+1\,l}) - \cdots), \tag{30}$$

where P_{ik} is a permutation operator and $P_{i_1 \cdots i_N} = P_{i_1 i_2} P_{i_2 i_3} \cdots P_{i_N i_1}$. Here we still label particles according to their position along the wire axis only: thus, nearest neighbors are particles in opposite rows whereas next-nearest neighbors are the closest particles within the same row. Note that for densities in the range $1.45 < \nu < 1.75$ the lateral displacement w is so large that the distance between nearest neighbors becomes larger than the distance between next-nearest neighbors.

Ring exchanges are interesting because they might stabilize a ferromagnetic ground state. While exchanges involving even numbers of particles favor a spin-zero ground state, exchanges involving odd numbers of particles favor a ferromagnetic arrangement of spins [45]. Thus, the simplest ring exchange process that could lead to a polarized ground state is the three-particle exchange. In fact, ring exchanges have been extensively studied in two-dimensional Wigner crystals [46–49]. In that case the three-particle ring exchange dominates in the low-density limit which implies a ferromagnetic ground state of the strongly interacting Wigner crystal in two dimensions[5]. To find out whether the physics of the zigzag Wigner crystal is similar, one needs to compute the exchange constants for nearest neighbor, next-nearest neighbor, and the various ring exchanges.

4.1. Computation of exchange constants

To introduce the method, we start by discussing the one-dimensional case where the only non-negligible exchange is the nearest-neighbor exchange.

4.1.1. Exchange constants for the one-dimensional Wigner crystal. The nearest-neighbor exchange constant J can be determined by computing the tunneling probability of two electrons through the Coulomb barrier that separates them. If the barrier is sufficiently high and, therefore, tunneling is weak, one may use the semiclassical instanton approximation. This corresponds to finding the classical exchange path in the inverted potential by minimizing the imaginary-time action.

It is convenient to rewrite the action in dimensionless form by rescaling length in units of $1/n$ and time in units of

[5] The ferromagnetic state is predicted to occur only at extremely low densities characterized by a value of $r_s > 175$ [49], where r_s is the ratio of the Coulomb interaction energy to the Fermi energy.

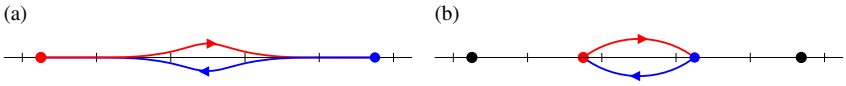

Figure 5. Sketch of typical exchange paths for (a) $\nu \ll \nu_c$ and (b) $\nu \lesssim \nu_c$. The size of the loop where electrons move away from the axis of the wire is determined by the length scale r_0.

$\sqrt{\epsilon m/e^2 n^3}$. The action of the system is then given as

$$S_{1D} = \frac{\hbar}{\sqrt{n a_B}} \eta_{1D}, \qquad \text{where}$$

$$\eta_{1D}[\{x_j(\tau)\}] = \int d\tau \left[\sum_j \frac{\dot{x}_j^2}{2} + \sum_{j<i} \frac{1}{|x_j - x_i|} \right]. \quad (31)$$

As a first approximation one may fix the positions of all particles except the two that participate in the exchange process, say $j = 1$ and 2. Symmetry fixes the center of mass coordinate of the exchanging electrons and, therefore, the minimization has to be done only with respect to the relative coordinate $x = x_2 - x_1$. The tunneling lifts the ground state degeneracy present due to inversion symmetry $x \to -x$, and the exchange energy can be identified with the resulting level splitting.

The instanton approximation yields the exchange constant J in the form (5), where η is the dimensionless classical action obtained from the minimization procedure. One finds $\eta \approx 2.817$ [50]. At low densities, $n a_B \ll 1$, the exponent is large leading to exponential suppression of J, and thus the prefactor omitted in (5) is of secondary importance.

Fixing the positions of all particles except the two participating in the exchange process is a somewhat crude approximation. Neighboring electrons see a modified potential due the motion of the exchanging particles and, therefore, experience a force that displaces them from their equilibrium positions. A better estimate for η can be obtained by including these mobile 'spectator' particles in the minimization. By allowing spectators to move during the exchange process, one expects to find a reduced value for η because more variables are varied in the minimization procedure. It turns out, however, that the effect is very small. As more spectators are added, η approaches the asymptotic value $\eta \approx 2.798$ [50–52], i.e., the result changes by less than 1%.

4.1.2. Exchange constants for the zigzag Wigner crystal. In the presence of a confining potential, the motion of the exchanging electrons is no longer restricted to one dimension, i.e., the position of an electron is now given by a two-dimensional vector $\mathbf{r}_j = (x_j, y_j)$. In particular, if the wire width W is larger than the Bohr's radius a_B or, equivalently, the interaction parameter introduced in equation (29) is large, $r_\Omega \gg 1$, electrons can make use of the transverse direction to go 'around' rather than 'through' each other during the exchange process. This reduces the Coulomb barrier and, therefore, increases the tunneling probability. The characteristic length scale of the transverse displacement is given by the length r_0, introduced in section 3. Typical trajectories for the one-dimensional crystal are shown in figure 5 for low and moderate densities, $\nu \ll \nu_c$ and $\nu \lesssim \nu_c$, respectively. At low densities, $\nu \ll \nu_c$, the exchange part follows the bottom of the confining potential until electrons come within a distance of order r_0 of each other. Thus, only a small part of the exchange path explores the transverse direction, leading to a relatively small correction to the tunneling action S_{1D}. The results of section 4.1.1 are recovered in the limit $\nu \to 0$. As one approaches the transition to the zigzag crystal, the exchange trajectories become more and more two-dimensional and consequently the exchange couplings are modified significantly. Finally, at $\nu > \nu_c$, also the equilibrium positions of the particles are displaced in the y-direction.

The exchange constants for the zigzag Wigner crystal can be obtained in the same way as for the one-dimensional Wigner crystal [53]. However, by contrast to the one-dimensional case, the structure of the zigzag crystal changes as a function of density. As a consequence the rescaling of lengths and times used in the one-dimensional case is not appropriate here. A dimensionless action in a transverse confining potential is conveniently defined using the interaction parameter r_Ω. Namely

$$S_{2D} = \hbar \sqrt{r_\Omega}\, \eta_{2D}, \qquad \text{where}$$

$$\eta_{2D}[\{\mathbf{r}_j(\tau)\}] = \int d\tau \left[\sum_j \left(\frac{\dot{\mathbf{r}}_j^2}{2} + y_j^2 \right) + \sum_{j<i} \frac{1}{|\mathbf{r}_j - \mathbf{r}_i|} \right]. \quad (32)$$

Here lengths have been rescaled in units of r_0 whereas times has been rescaled in units of $\sqrt{2}/\Omega$. Furthermore, comparing (31) and (32), the differences are the one-dimensional vs two-dimensional coordinates and the additional term due to the confining potential in (32).

As a result the exchange constants take the form

$$J_l = J_l^* \exp\left(-\eta_l \sqrt{r_\Omega}\right), \quad (33)$$

where J_1 is the nearest-neighbor exchange constant, J_2 is the next-nearest neighbor exchange constant, and J_l for $l \geqslant 3$ is the exchange constant corresponding to the l-particle ring exchange. The exponents η_l are obtained by minimizing the dimensionless action $\eta_{2D}[\{\mathbf{r}_j(\tau)\}]$ for a given exchange process. Whereas in the strictly one-dimensional case η was just a number, now the electron configuration changes as a function of density and, therefore, the exponents η_l depend on density, too.

Note that while in the one-dimensional case the inclusion of spectators had little effect on the results, here the spectators turn out to be much more important [53]. Figure 6(a) shows the change of the exponents η_l as spectators are included. As one can see, the first few spectators modify the results significantly. However, the results converge rapidly as more and more spectators are added. Thus, the spin couplings are generated by

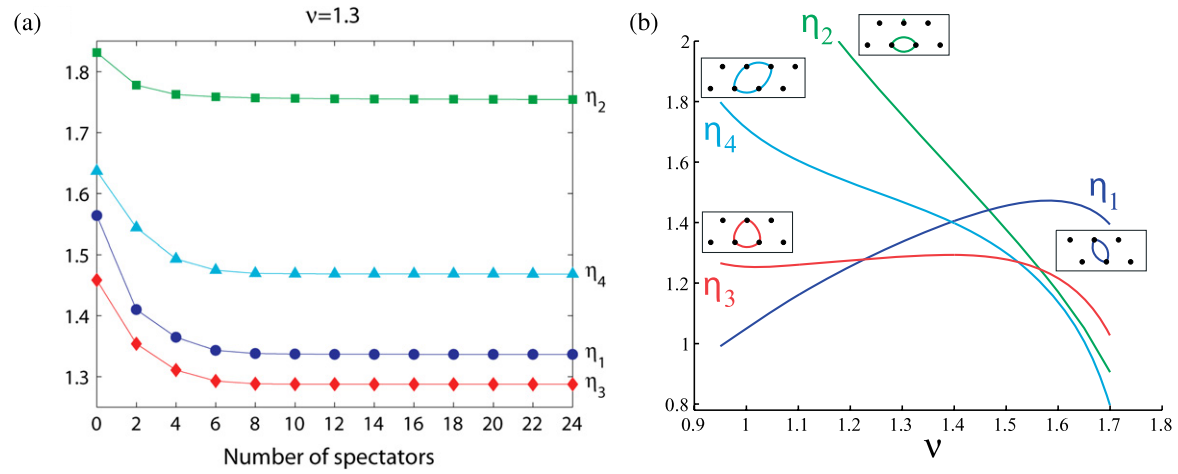

Figure 6. (a) Dependence of the exponents η_l on the number of spectators included in the calculation [54]. Results are shown for $\nu = 1.3$. (b) Exponents η_l for the nearest neighbor, next-nearest neighbor, three-particle ring, and four-particle ring exchange as a function of dimensionless density ν [55].

processes that involve the motion of a small number of close-by electrons. Therefore, these couplings should not be affected by deviations from the perfect crystalline order at large distances, caused by quantum fluctuations.

Figure 6(b) shows the exponents η_l as a function of the dimensionless density ν [53, 55]. Ring exchanges with more than four particles are not included as they are negligibly small at all densities. At small $\nu \lesssim 1.2$, the crystal geometry is still close to one-dimensional. In that regime η_1 is the smallest exponent and therefore, as expected, the nearest-neighbor exchange J_1 dominates. However, as density increases and the distances between nearest neighbors and next-nearest neighbors become comparable, in the regime $1.2 \lesssim \nu \lesssim 1.5$ the three-particle ring exchange constant J_3 becomes largest. Finally, at even higher densities $\nu \gtrsim 1.5$ the four-particle ring exchange is dominant (until the zigzag crystal gives way to structures with more than two rows at $\nu \approx 1.75$). In the next section the ground states generated by these spin couplings will be discussed.

4.2. Spin phases of the zigzag Wigner crystal

In order to extract the spin properties of the ground state, it is convenient to rewrite Hamiltonian (30) in terms of spin operators using the identity $P_{ik} = \frac{1}{2} + 2\,\boldsymbol{S}_i \cdot \boldsymbol{S}_k$. In the absence of ring exchanges the system is described as a Heisenberg spin chain with nearest neighbor and next-nearest neighbor coupling,

$$H_{12} = \sum_l \left(J_1\,\boldsymbol{S}_l \cdot \boldsymbol{S}_{l+1} + J_2\,\boldsymbol{S}_l \cdot \boldsymbol{S}_{l+2}\right). \tag{34}$$

As discussed at the beginning of this section, depending on the ratio of J_1 and J_2, one finds an antiferromagnetic and a dimer phase. The contribution of the three-particle ring exchange is

$$H_3 = -J_3 \sum_l \left(2\boldsymbol{S}_l \cdot \boldsymbol{S}_{l+1} + \boldsymbol{S}_l \cdot \boldsymbol{S}_{l+2}\right). \tag{35}$$

Thus, no new terms are generated—the Hamiltonian retains the same form (34), albeit with modified coupling constants

$$\widetilde{J}_1 = J_1 - 2J_3, \qquad \widetilde{J}_2 = J_2 - J_3. \tag{36}$$

The important consequence is that the new coupling constants $\widetilde{J}_1$ and $\widetilde{J}_2$ may now be either positive or negative, corresponding to antiferromagnetic or ferromagnetic interactions, respectively. The phase diagram of a Heisenberg spin chain with both antiferromagnetic and ferromagnetic nearest and next-nearest neighbor couplings has been widely studied in the literature [40–44, 56–61]. In addition to the antiferromagnetic and dimer phases existing for positive couplings, a ferromagnetic phase appears. The phase diagram is shown in figure 7(a).

This phase diagram is sufficient to determine the ground state of the strongly interacting zigzag Wigner crystal at low and intermediate densities. At low densities, the system is in the antiferromagnetic phase ($\widetilde{J}_1 > 0$, $|\widetilde{J}_2| \ll \widetilde{J}_1$). At intermediate densities, the three-particle ring exchange dominates. As a result both coupling constants become negative, $\widetilde{J}_1, \widetilde{J}_2 < 0$, and therefore the system is in the ferromagnetic phase. The spontaneous spin polarization suggested as a possible explanation of the 0.7 structure can, thus, occur in strongly interacting quantum wires, if deviations from one-dimensionality are taken into account.

At higher densities, the situation becomes more complicated. While the three-particle ring exchange only modifies the nearest neighbor and next-nearest neighbor exchange constants, the four-particle ring exchange generates new terms in the Hamiltonian, namely a next-next-nearest neighbor exchange and, more importantly, four-spin couplings. The corresponding spin Hamiltonian reads

$$H_4 = J_4 \sum_l \Bigg(\sum_{n=1}^{3} \frac{4-n}{2} \boldsymbol{S}_l \cdot \boldsymbol{S}_{l+n} + 2[(\boldsymbol{S}_l \cdot \boldsymbol{S}_{l+1})(\boldsymbol{S}_{l+2} \cdot \boldsymbol{S}_{l+3}) + (\boldsymbol{S}_l \cdot \boldsymbol{S}_{l+2})(\boldsymbol{S}_{l+1} \cdot \boldsymbol{S}_{l+3}) - (\boldsymbol{S}_l \cdot \boldsymbol{S}_{l+3})(\boldsymbol{S}_{l+1} \cdot \boldsymbol{S}_{l+2})] \Bigg). \tag{37}$$

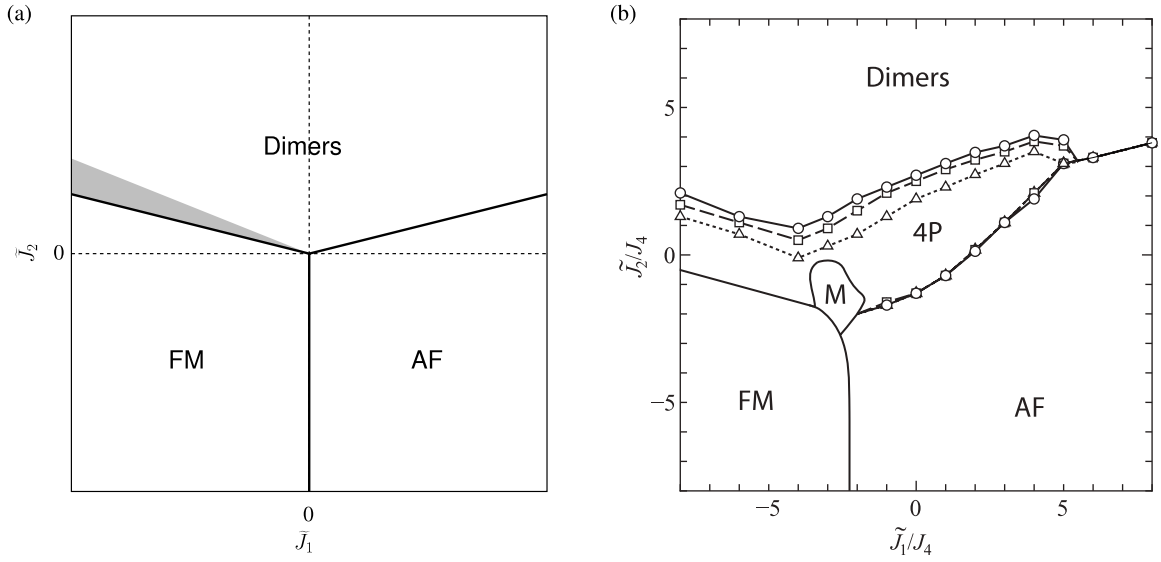

Figure 7. (a) Phase diagram of the Heisenberg spin chain with nearest-neighbor coupling $\widetilde{J}_1$ and next-nearest neighbor coupling $\widetilde{J}_2$. (b) Preliminary phase diagram of the zigzag spin chain including four-particle ring exchange J_4, obtained by exact numerical diagonalization of finite-size chains [55]. When J_4 is large, novel phases appear. (Triangles, squares, and circles correspond to the boundaries obtained for $N = 16$, 20, and 24 sites, respectively.)

The phase diagram in the presence of these couplings is not yet fully understood. First results were obtained using exact diagonalization of short chains with up to $N = 24$ spins [55]. If $J_4 \ll |\widetilde{J}_1|, |\widetilde{J}_2|$, the same phases as in the Heisenberg spin chain without four-particle ring exchange appear as can be seen in figure 7(b). However, as J_4 becomes of the same order as the other coupling constants new phases appear. The simplest one to identify is a partially polarized phase (labeled 'M' in figure 7(b)) adjacent to the ferromagnetic phase. While this phase seems to persist in size and shape as the number of spins increases, it is currently unclear whether it survives in the thermodynamic limit. In addition a region (labeled '4P' in figure 7(b)) where the ground state is unpolarized but different from the antiferromagnetic and dimer phases occurs. This '4P' region could correspond to a single or several phases. Unfortunately, the size dependence in this part of the phase diagram turns out to be very complicated. Due to frustration introduced by the four-particle exchange, a large number of low-energy states exist. Therefore, the study of short chains does not allow one to determine the properties of the ground state in this regime.

4.3. Spin phases of interacting quantum wires in the quasi-one-dimensional regime

While the above results were obtained in the limit $r_\Omega \gg 1$, interaction parameters in realistic quantum wires vary widely, ranging from $r_\Omega < 1$ in cleaved-edge overgrowth wires to $r_\Omega \approx 20$ in p-type gate-defined wires [62–64]. While the former are weakly interacting, the latter are clearly in the strongly interacting regime. However, the above analysis based solely on exponents is not sufficient to determine the ground state of interacting electrons in a quantum wire at finite r_Ω. In order to obtain a phase diagram in that case, the prefactors J_l^* have to be computed which can be done by including Gaussian fluctuations around the classical exchange paths.

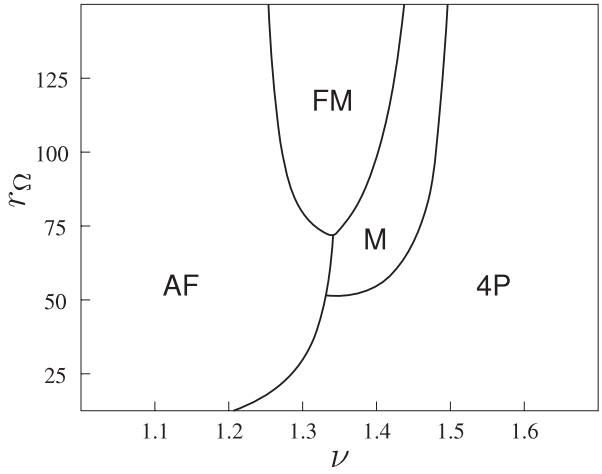

Figure 8. Spin ground states of interacting electrons in quantum wires in the zigzag regime [55].

Using the exchange constants $J_l(\nu, r_\Omega)$ computed in this way [55] and the phase diagram shown in figure 7, the ground states realized for given system parameters can be determined. The resulting phase diagram is shown in figure 8. It turns out that the partially and fully polarized phases are realized only at large $r_\Omega \gtrsim 50$. At moderately large r_Ω the transition occurs directly from the antiferromagnetic phase to a phase dominated by the four-particle ring exchange. These findings, thus, do not support the interpretation [12–18, 20–25] of the so-called 0.7 structure in terms of spontaneous spin polarization.

Even at sufficiently strong interactions, the question arises of how a ferromagnetic state in the quantum wire manifests itself in the conductance. It is tempting to assume that in

the fully polarized state the wire supports only one excitation mode and thus has conductance e^2/h. This is indeed the case when the full polarization of electron spins is achieved by applying a sufficiently strong magnetic field. Such a field creates a gap in the spectrum of spin excitations, and below the gap the system is equivalent to a spinless electron liquid with conductance e^2/h. It is important to stress that the situation is very different if the full spin polarization is achieved due to internal exchange processes in the electron system, rather than the external magnetic field. In this case, the ground state is degenerate with respect to spin rotations, and thus the system supports gapless spin excitations—the magnons. As a result, the conventional argument in favor of conductance value e^2/h no longer applies.

In studying the conductance of a ferromagnetic wire it is important to keep in mind that the properties of the electron system inside the quantum wire in general do not fully determine its conductance. Indeed, since the electric current flows between non-magnetic leads through a ferromagnetic wire, the spatial non-uniformity of the system needs to be considered carefully, and the problem of determining the conductance complicates considerably. In the case of a ferromagnetic zigzag Wigner crystal in the middle of the wire, the weakening of the confining potential in the contact region would lead to either melting of the crystal or the emergence of a crystal with more and more rows. In both cases modeling of the spin interactions in the transition region is by no means obvious.

The simplest model that might capture the relevant physics is one where the system is described by Hamiltonian (4) with an effective position-dependent nearest-neighbor exchange constant $J(x)$ as depicted in figure 9. In the leads, interactions are weak and antiferromagnetic and therefore J is large and positive. In the wire, interactions are strong and ferromagnetic and therefore J is small and negative. Through the contact regions, J varies smoothly and changes sign at points $-a$ and a. Within this model, the arguments of section 2.3 lead to the conclusion that the spin polarization does suppress the conductance. Namely, since the exchange coupling constant vanishes at the borders of the ferromagnetic region, i.e., at $\pm a$, the spin degrees of freedom in the leads are decoupled from those in the wire and, thus, the propagation of spin excitations through the wire is blocked. Accordingly, the value of the conductance is reduced by a factor 2. By contrast to the antiferromagnetic case in one-dimensional wires, this suppression would persist down to temperatures $T \to 0$ due to the vanishing of the spin coupling in the contact region.

Of course the contact region in real quantum wires is more complex and a satisfactory theory for the conductance of strongly interacting quasi-one-dimensional quantum wires that correctly takes into account the spin degrees of freedom is an open problem.

5. Orbital properties of zigzag Wigner crystals

In addition to the spin physics discussed in the previous section, quasi-one-dimensional wires have interesting orbital properties. In this section, we discuss the transition from a one-dimensional to a quasi-one-dimensional state for the case of spinless electrons, based mainly on [65].

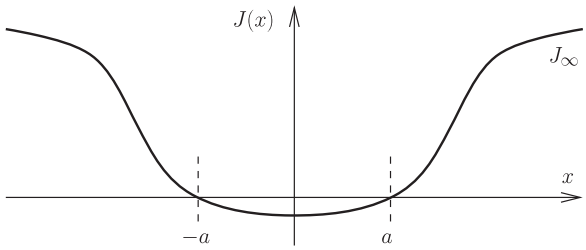

Figure 9. Simple model of exchange coupling in a ferromagnetic Wigner crystal coupled to non-magnetic leads. The coupling constant vanishes in the contact region at points $-a$ and a, and therefore the spin excitations in the leads and in the wire decouple.

As shown in section 3, the classical transition from a one-dimensional to a zigzag Wigner crystal can be obtained simply by minimizing the energy of the interacting electron system in a transverse confining potential. A different way of studying the same transition is by considering the phonon modes of the crystal. In the one-dimensional crystal one longitudinal and one transverse phonon mode exist. The longitudinal phonon is gapless because sliding of the entire crystal along the wire axis does not cost any energy. On the other hand, the transverse mode is gapped with a gap frequency equal to the frequency of the confining potential. The transition to a zigzag state is driven by a softening of the transverse phonon at wavevector $k = \pi n$ which corresponds to a staggered displacement of electrons transverse to the wire axis. In the zigzag crystal, we obtain two longitudinal and two transverse phonon modes with the following low-q dispersions [66] close to the transition ($\delta\nu/\nu \ll 1$):

$$\omega_{\parallel 0}(q) = \frac{\pi}{2}\,\Omega\sqrt{\nu_c^3 \ln\frac{1}{|q|}}\;|q|, \qquad (38)$$

$$\omega_{\parallel \pi}(q) = \sqrt{2}\,\Omega + \mathcal{O}(q^2),$$

$$\omega_{\perp 0}(q) = \Omega + \mathcal{O}(q^2),$$

$$\omega_{\perp \pi}(q) = \sqrt{6}\,\Omega\sqrt{\frac{\delta\nu}{\nu_c} + \frac{\pi^2 \ln 2}{48}\nu_c^3\, q^2}, \qquad (39)$$

where $q = k/(\pi n)$.

Thus, only at the transition point $\delta\nu = 0$, two gapless phonon modes exist with dispersions $\omega_{\parallel 0}(q)$ and $\omega_{\perp\pi}(q) = (\pi/2\sqrt{2})\,\Omega\sqrt{\nu_c^3 \ln 2}\,|q|$. Within the zigzag regime, there is a single gapless excitation corresponding to in-phase longitudinal motion of the two rows that constitute the zigzag crystal. The soft-mode $\omega_{\perp\pi}(q)$ describing the out-of-phase transverse motion acquires a gap $\Delta_{\rm cl} \propto \sqrt{\delta\nu}$.

This behavior is markedly different from the noninteracting case. In a noninteracting system the transition from a one-dimensional to a quasi-one-dimensional state happens when the chemical potential is raised above the subband energy of the second subband of transverse quantization. In the quasi-one-dimensional state, the two occupied subbands are decoupled and each of them supports a gapless electronic excitation

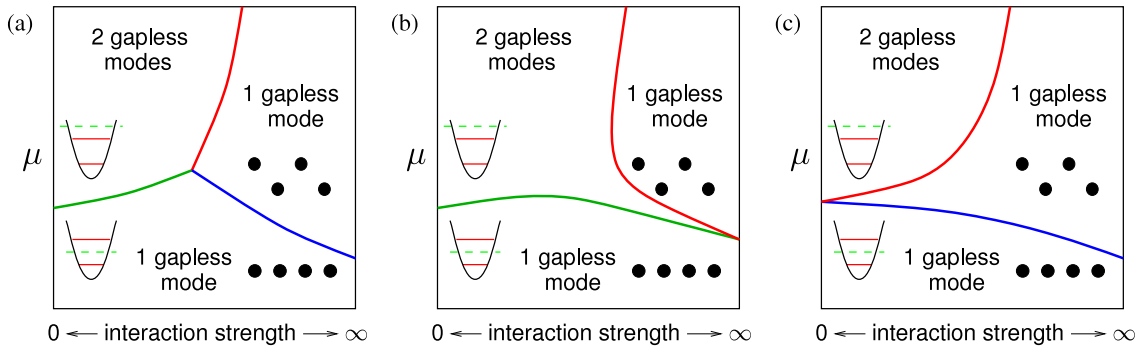

Figure 10. At zero and infinite interaction strength the quasi-one-dimensional system supports two and one gapless excitation mode, respectively. Here the interaction strength is characterized by the parameter r_Ω introduced in section 3. Possible phase diagrams consistent with these findings are shown: (a) a tricritical point exists at a finite interaction strength. (b) Weak quantum fluctuations destroy the gap of the classical Wigner crystal. (c) Already infinitesimally weak interactions induce a gap in the second mode.

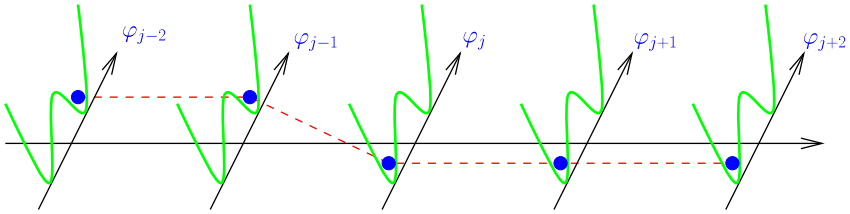

Figure 11. Mapping of the φ^4-theory to a spin chain.

mode, i.e., above the transition two gapless modes exist rather than just one as in the classical Wigner crystal.

One might, thus, expect that the phase diagram of the system as a function of interaction strength is as shown in figure 10(a), namely two distinct quasi-one-dimensional phases exist at weak and strong interactions. Consequently one should find a tricritical point at a finite interaction strength where the nature of the transition from a one-dimensional to a quasi-one-dimensional state changes. However, the phase diagram figure 10(a) is not the only one consistent with both the above findings for the noninteracting case and the classical Wigner crystal at infinite interaction strength. Two alternatives are shown in figures 10(b) and (c). To distinguish between the different possibilities, one needs to study the nature of the transition as a function of interaction strength. In particular, the following questions have to be answered: (i) do weak quantum fluctuations destroy the gap found in the classical zigzag crystal at strong interactions? (ii) Do infinitesimally weak interactions lead to a gap in the second mode above the transition?

5.1. Quantum theory of the zigzag transition

Let us consider the strongly interacting case first and account for the quantum nature of the system. In particular, using the classical Wigner crystal configuration as a starting point, we now include quantum fluctuations. The phonon modes (38) and (39) reflect the fact that there are only two types of possible low-energy excitations: the longitudinal plasmon mode and a staggered transverse mode. It turns out that in the vicinity of the transition the two modes decouple. The acoustic spectrum of the plasmon mode is protected by translational invariance and, thus, at least one gapless excitation mode exists in the system. More interesting is the staggered transverse mode.

To describe the transverse displacements of the electrons, a staggered field $\varphi_l = (-1)^l y_l$ is introduced. In the vicinity of the transition, φ_l is slowly varying on the scale of the inter-electron distances and, therefore, the continuum limit $\varphi_l \to \varphi(x)$ can be taken. Expanding the action up to fourth order in φ, one finds

$$S[\varphi] = A\hbar\sqrt{r_\Omega}\int \mathrm{d}\tau\,\mathrm{d}x\,\left[(\partial_\tau\varphi)^2 + (\partial_x\varphi)^2 - \delta\nu\,\varphi^2 + \varphi^4\right], \tag{40}$$

where the variables have been rescaled such as to provide the simplest action possible. The form of the action as well as all following conclusions do not depend on the exact shape of the confining potential. For a parabolic confining potential the constant A is given as $A = [7\zeta(3)]^{3/2}\sqrt{\ln 2}/(31\zeta(5))$.

The classical transition point as discussed above corresponds to $\delta\nu = 0$. Here the transverse mode becomes unstable, and the quartic term is needed to stabilize the system. Quantum fluctuations may affect both the transition point and the nature of the transition. A convenient way to analyze the quantum-mechanical problem is to refermionize. As a first step, we rediscretize the coordinate x along the wire axis. The discrete version of the Hamiltonian then describes a set of particles moving in a double-well potential $V_{\mathrm{DW}} \sim -\lambda\varphi_j^2 + \varphi_j^4$ (as depicted in figure 11) and interacting through a nearest-neighbor interaction $\propto(\varphi_j - \varphi_{j+1})^2$. If the double-well potential is sufficiently deep, i.e., if λ is sufficiently large, the particles are almost completely localized in one of the wells at $\varphi_j = \pm\sqrt{\lambda/2}$. Then each particle can be described

by a pseudo-spin operator, namely $\varphi_j = \sqrt{\lambda/2}\,\sigma_j^z$, where σ_j^z is a Pauli matrix. In terms of these new variables, the Hamiltonian consists of two terms corresponding to tunneling between the two wells and the nearest-neighbor interaction, respectively. Tunneling is described by $H_t = -t\sum_j \sigma_j^x$ whereas the interaction term reads $H_{\rm NN} = -v\sum_j \sigma_j^z\sigma_{j+1}^z$. The resulting Hamiltonian $H_t + H_{\rm NN}$ is the Hamiltonian of the transverse field Ising model [67]. Here the parameters t and v are related to the parameters of the original model. In particular, they can be tuned by changing the chemical potential which controls the transition, i.e., $t = t(\mu)$ and $v = v(\mu)$.

In order to arrive at a fermionic description, a Jordan–Wigner transformation is used. It turns out that the Hamiltonian takes a much simpler form if one rotates $\sigma^x \to -\sigma^z$ first. The representation of the spin operators in terms of (spinless) fermions,

$$\sigma_j^+ \equiv \sigma_j^x + i\sigma_j^y = 2a_j^\dagger e^{i\pi\sum_{i<j} a_i^\dagger a_i},$$
$$\sigma_j^- \equiv \sigma_j^x - i\sigma_j^y = 2e^{-i\pi\sum_{i<j} a_i^\dagger a_i} a_j, \qquad \sigma_j^z = 2a_j^\dagger a_j - 1, \tag{41}$$

where $a_j^\dagger$ and a_j are fermion creation and annihilation operators on site j, respectively, then yields the noninteracting Hamiltonian [67]

$$H_{\rm f} = \sum_j [2t\, a_j^\dagger a_j - v(a_j^\dagger - a_j)(a_{j+1}^\dagger + a_{j+1})]. \tag{42}$$

Note that this Hamiltonian is essentially the transfer matrix of the two-dimensional classical Ising model [68] near the transition. The connection can be made clear by considering the mapping between d-dimensional quantum and $(d+1)$-dimensional classical models [69]. Thus, the one-dimensional quantum Ising model studied here is equivalent to the two-dimensional classical Ising model [70].

In Hamiltonian (42) one can identify three different contributions: $-v(a_j^\dagger a_{j+1} + a_{j+1}^\dagger a_j)$ describes a tight-binding model with bandwidth $4v$, the local term $2ta_j^\dagger a_j$ yields the chemical potential $\mu_{\rm f} = -2t$ of the spinless fermions, figure 12, and finally $-v(a_j^\dagger a_{j+1}^\dagger - a_j a_{j+1})$ is a BCS-like pairing term with p-wave symmetry. The one-dimensional regime of our original model corresponds to $t > v$ when the chemical potential lies below the bottom of the tight-binding band and, therefore, all the fermionic states are empty. The transition to a quasi-one-dimensional regime happens when the chemical potential reaches the bottom of the band at $t = v$. For $t < v$, some of the fermionic states describing the motion of the original electrons transverse to the wire axis are filled. Due to the pairing term in the Hamiltonian, these states acquire a gap. With the help of a Bogoliubov transformation, the Hamiltonian can be diagonalized to obtain the energy spectrum. As a result one finds that the gap is given as $\Delta = 2|t - v|$.

In terms of the original system parameters, one expects that t and v are non-singular functions of the chemical potential. The critical chemical potential $\mu_{\rm c}$ is thus defined by the condition $t(\mu_{\rm c}) = v(\mu_{\rm c})$. Furthermore, the behavior of the gap is obtained by expanding $t - v$ in the vicinity of the transition point $\mu_{\rm c}$. As a consequence one obtains a linear gap,

$$\Delta \propto |\mu - \mu_{\rm c}|. \tag{43}$$

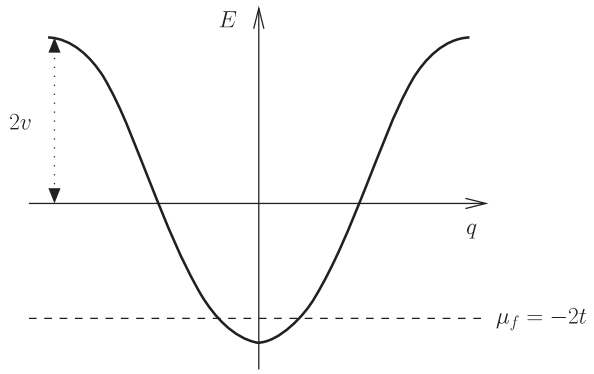

Figure 12. After the Jordan–Wigner transformation, one obtains a tight-binding model for spinless fermions with bandwidth $2v$ and chemical potential $-2t$. The transition from a one-dimensional to a quasi-one-dimensional state happens when the chemical potential reaches the bottom of the band.

While quantum effects modify the nature of the transition, the number of gapless excitations remains the same: in the strongly interacting system, only one gapless excitation exists. Thus, the phase diagram of figure 10(b) is ruled out—weak quantum fluctuations do not destroy the gap of the transverse mode in the quasi-one-dimensional regime. To differentiate between the phase diagrams of figures 10(a) and (c), a complementary approach has to be used. In section 5.2 we consider the limit of weak interactions to check whether or not they lead to the formation of a gap just above the transition, as suggested by the scenario of figure 10(c).

5.2. Two-subband system at weak interactions

The limit of weak interactions can be treated using a renormalization group approach. Here the description in terms of two subbands due to transverse size quantization is a good starting point. Each subband is described by fermionic operators ψ_j, where $j = 1, 2$. The free Hamiltonian is just

$$H_0 = \sum_j \int {\rm d}x \left[-\frac{\hbar^2}{2m}\psi_j^\dagger \partial^2 \psi_j + \varepsilon_j \psi_j^\dagger \psi_j\right], \tag{44}$$

where ε_j are the subband energies. For a parabolic confining potential, $\varepsilon_j = \hbar\Omega(j - \frac{1}{2})$.

Interactions can be separated into intra-subband and inter-subband interactions. One needs four interaction constants to describe the system: $g_j \sim V_{jj}(0) - V_{jj}(2k_{{\rm F}j})$ which describes intra-subband forward scattering,

$$g_x \sim V_{12}(0) - \tfrac{1}{2}(V_{12}^{\rm ex}(k_{\rm F1} - k_{\rm F2}) + V_{12}^{\rm ex}(k_{\rm F1} + k_{\rm F2})) \tag{45}$$

which describes inter-subband forward scattering, and

$$g_t \sim V_{12}^{\rm ex}(k_{\rm F1} - k_{\rm F2}) - V_{12}^{\rm ex}(k_{\rm F1} + k_{\rm F2}) \tag{46}$$

which describes transfer of two particles between the subbands

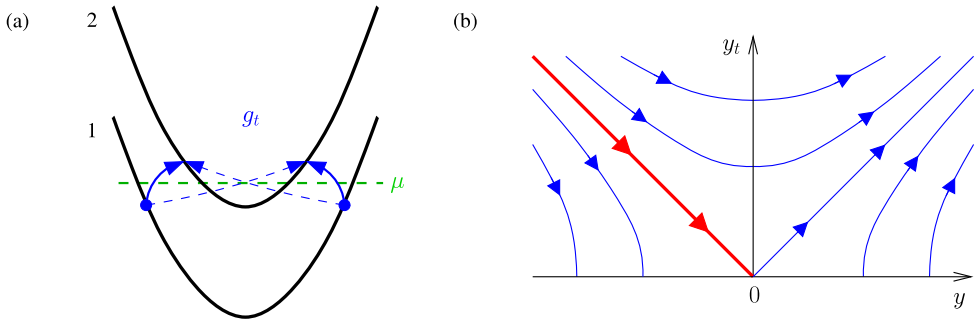

Figure 13. (a) Two-particle transfer between subbands described by the coupling constant g_t. (b) Weak coupling RG flow.

as shown in figure 13(a). Here

$$V_{ij}(k) = \int \mathrm{d}x\, \mathrm{d}x'\, \mathrm{e}^{\mathrm{i}k(x-x')} \times \int \mathrm{d}y\, \mathrm{d}y'\, V_{\mathrm{int}}(\mathbf{r}-\mathbf{r}')\chi_i^2(y)\chi_j^2(y'), \tag{47}$$

$$V_{ij}^{\mathrm{ex}}(k) = \int \mathrm{d}x\, \mathrm{d}x'\, \mathrm{e}^{\mathrm{i}k(x-x')} \times \int \mathrm{d}y\, \mathrm{d}y'\, V_{\mathrm{int}}(\mathbf{r}-\mathbf{r}')\chi_i(y)\chi_j(y)\chi_i(y')\chi_j(y'), \tag{48}$$

where χ_i are the transverse eigenmodes in the confining potential.

It is well known that forward scattering in one dimension does not open a gap in the system [7]. By contrast, the two-particle transfer between subbands described by the coupling constant g_t could open a gap. To assess whether this is indeed the case, the renormalization group (RG) is used, i.e., reducing the bandwidth from D_0 down to D, the scale-dependent coupling constants are determined. The RG equations for a two-band system are given as [71–73]

$$g_1' = -\frac{1}{2\pi\hbar v_{\mathrm{F2}}} g_t^2, \qquad g_2' = -\frac{1}{2\pi\hbar v_{\mathrm{F1}}} g_t^2, \qquad g_x' = \frac{1}{\pi\hbar(v_{\mathrm{F1}}+v_{\mathrm{F2}})} g_t^2, \tag{49}$$

$$g_t' = -\frac{1}{2\pi\hbar}\left(\frac{g_1}{v_{\mathrm{F1}}} + \frac{g_2}{v_{\mathrm{F2}}} - \frac{4g_x}{v_{\mathrm{F1}}+v_{\mathrm{F2}}}\right) g_t, \tag{50}$$

where the derivatives are taken with respect to $\xi = \ln(D_0/D)$. By introducing the dimensionless coupling constants

$$y = -\frac{1}{2\pi\hbar}\left(\frac{g_1}{v_{\mathrm{F1}}} + \frac{g_2}{v_{\mathrm{F2}}} - \frac{4g_x}{v_{\mathrm{F1}}+v_{\mathrm{F2}}}\right), \qquad y_t = \frac{g_t}{\pi\hbar}\sqrt{\frac{(v_{\mathrm{F1}}+v_{\mathrm{F2}})^2 + 4v_{\mathrm{F1}}v_{\mathrm{F2}}}{2v_{\mathrm{F1}}v_{\mathrm{F2}}(v_{\mathrm{F1}}+v_{\mathrm{F2}})^2}}, \tag{51}$$

the four RG equations can be combined into two equations [73]

$$y' = y_t^2, \qquad y_t' = y y_t. \tag{52}$$

The flow diagram corresponding to these equations is shown in figure 13(b).

The coupling constant g_t describes a combination of two processes: the particles transferred between subbands may retain their direction of motion, corresponding to momentum transfer $\pm(k_{\mathrm{F1}} - k_{\mathrm{F2}})$, or they may change their direction of motion, corresponding to momentum transfer $\pm(k_{\mathrm{F1}} + k_{\mathrm{F2}})$. Both processes are depicted in figure 13(a). The resulting coupling constant, thus, is proportional to $V_{12}^{\mathrm{ex}}(k_{\mathrm{F1}} - k_{\mathrm{F2}}) - V_{12}^{\mathrm{ex}}(k_{\mathrm{F1}} + k_{\mathrm{F2}})$ as given in equation (46). Consequently, $g_t^{(0)} \propto k_{\mathrm{F2}}$ as the density in the second subband goes to zero, and one concludes that $y_t^{(0)} \propto \sqrt{v_{\mathrm{F2}}}$ is much smaller that $y^{(0)}$. Therefore the presence or absence of a gap just above the transition to a quasi-one-dimensional state is determined by the sign of $y^{(0)}$. If $y^{(0)} < 0$, the coupling constant y_t flows to zero, and the system remains gapless. On the other hand, if $y^{(0)} > 0$, the coupling constant y_t flows to infinity, and the system acquires a gap.

The interaction constant $y^{(0)}$ can be evaluated assuming a Coulomb interaction screened by a gate at a distance d much larger than the effective width of the wire, i.e.,

$$V_{\mathrm{int}}(r) = \frac{e^2}{2\epsilon}\left(\frac{1}{r} - \frac{1}{\sqrt{r^2+(2d)^2}}\right) \tag{53}$$

which is the two-dimensional version of equation (1).

One finds that $g_1 \approx g_x \approx 2(e^2/\epsilon)\ln k_{\mathrm{F1}} d$ (with logarithmic accuracy). On the other hand, at densities $n_2 \ll 1/d$,

$$g_2 \sim \frac{e^2}{\epsilon}(k_{\mathrm{F2}}d)^2 \ln\frac{1}{k_{\mathrm{F2}}d}, \tag{54}$$

i.e., the interaction constant g_2 vanishes in the limit $n_2 \to 0$. This is a manifestation of the Pauli exclusion principle: once the average distance between particles exceeds the distance to the gate, the interactions become effectively local. However, identical fermions do not interact via a local interaction, hence $g_2 \to 0$.

Using the above expressions for the interaction constants, one finds the initial value $y^{(0)} \approx 3g_1/(2\pi\hbar v_{\mathrm{F1}}) > 0$. As $y^{(0)}$ is positive, the system flows to strong coupling. Thus, the system develops a gap close to the transition from a one-dimensional to a quasi-one-dimensional state, and therefore the phase diagram figure 10(a) does not describe the system.

A second gapless excitation mode appears only once the density is increased further beyond the transition point. As the density increases, g_2/v_{F2} increases and becomes comparable to g_1/v_{F1}. Then $y^{(0)}$ changes sign and eventually one crosses into the regime where y_t scales to zero. At weak interactions this

happens at $k_{F2} \sim 1/(k_{F1}d^2)$. Thus, at any interaction strength there is a finite window of densities in which the system is in the quasi-one-dimensional state but supports only one gapless excitation mode. The resulting phase diagram [65] is shown in figure 14.

Having found that the behavior at weak and strong interactions is very similar, there is no reason to expect that at intermediate interactions no gap exists. One notices, however, that the magnitude of the gap strongly depends on interaction strength. In the Wigner crystal we find a large Ising gap $\Delta \sim |\delta\mu|$. At weak interactions, on the other hand, the gap scales with a large exponent, $\Delta \sim (\delta\mu)^\alpha$, where $\alpha = 1/(4y^{(0)})$.

5.3. Intermediate interactions

The method of choice to treat intermediate interactions in one-dimensional and quasi-one-dimensional systems is bosonization. However, bosonization requires a linear spectrum. In the present case this is not straightforward because, to describe the transition, one is necessarily interested in what happens at the bottom of the second subband where a linearization is not justified.

Alternatively one may bosonize the first subband which has a large Fermi energy and keep a fermionic description in the second subband [74]. Thus, the electrons in the first subband are described by the bosonic fields $\phi_1(x)$ and $\theta_1(x)$ whereas the electrons in the second subband are described by the fermionic creation and annihilation operators, $\psi_2^\dagger(x)$ and $\psi_2(x)$. In particular,

$$\begin{aligned} H = {} & \frac{\hbar v_{F1}}{2\pi}\int \mathrm{d}x\,\left((\partial\theta_1)^2 + \frac{1}{K^2}(\partial\phi_1)^2\right) \\ & - \frac{\hbar^2}{2m}\int \mathrm{d}x\;\psi_2^\dagger\partial^2\psi_2 \\ & - \frac{1}{\pi}\sum_q (\partial\phi_1)(q)V_{12}(q)n_2(-q) \\ & + \gamma_t\int \mathrm{d}x\,[(\psi_2^\dagger\partial\psi_2^\dagger - \partial\psi_2^\dagger\psi_2^\dagger)\mathrm{e}^{-2\mathrm{i}\theta_1} + \mathrm{h.c.}], \end{aligned} \tag{55}$$

where $\gamma_t \sim e^2/\epsilon$. Furthermore, $K = (1 + g_1/\pi\hbar v_{F1})^{-1/2}$ is the Luttinger parameter in the first subband.

The dominant interaction between the bosons and the fermions is the inter-subband forward scattering V_{12}. This coupling can be eliminated by applying a unitary transformation

$$U = \exp\left[-\frac{\mathrm{i}K^2}{\pi\hbar v_{F1}}\int \mathrm{d}x\,\mathrm{d}y\;\theta_1(x)V(x-y)n_2(y)\right]. \tag{56}$$

The new Hamiltonian in terms of the transformed bosonic (ϕ_c, θ_c) and fermionic $(\psi_s^\dagger, \psi_s)$ fields then reads

$$\begin{aligned} H_U = {} & UHU^\dagger \\ = {} & \frac{\hbar v_{F1}}{2\pi}\int \mathrm{d}x\,\left((\partial\theta_c)^2 + \frac{1}{K^2}(\partial\phi_c)^2\right) - \frac{\hbar^2}{2m}\int \mathrm{d}x\;\psi_s^\dagger\partial^2\psi_s \\ & + \gamma_t\int \mathrm{d}x\,\left[(\psi_s^\dagger\partial\psi_s^\dagger - \partial\psi_s^\dagger\psi_s^\dagger)\mathrm{e}^{-2\mathrm{i}\kappa\theta_c(x)} + \mathrm{h.c.}\right], \end{aligned} \tag{57}$$

i.e., the inter-subband forward scattering disappears. Comparing the Hamiltonians (55) and (57), note that the exponent in the boson–fermion interaction term changes from $2\mathrm{i}\theta_c$ to $2\mathrm{i}\kappa\theta_c$, where $\kappa = 1 - K^2 g_x/(\pi\hbar v_{F1}) \simeq K^2$. It is essential to realize that other than that the Hamiltonian preserves its form after the unitary transformation. Namely we are still dealing with a plasmon mode coupled to noninteracting fermions. Not only the bare interaction in the second subband, but also the effective interaction generated by the inter-subband forward scattering vanishes in the limit $n_2 \to 0$. Additional terms that are generated by the unitary transformation can be shown to be irrelevant [74].

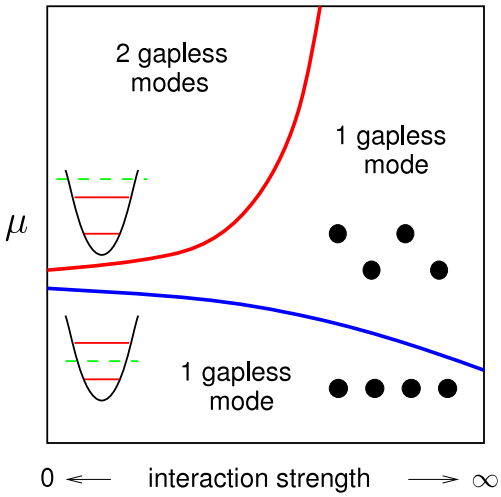

Figure 14. Phase diagram of spinless interacting electrons in a quantum wire [65]. At any interaction strength there is a finite window of densities where the quasi-one-dimensional system supports only one gapless excitation.

Since the fermions remain noninteracting, as a next step, they can be bosonized. The purely bosonic Hamiltonian could then in principle be subject to an RG approach. Or, as it is safe to assume that at intermediate interactions the second mode is still gapped, one may use a variational approach instead. One finds that the gap exponent decreases with increasing interaction strength until the variational approach is no longer valid because the relevant energy scale exceeds the Fermi energy in the second subband [66]. For stronger interactions, note that the Hamiltonian (57) in the limit $K \to 0$ takes the same form as the Hamiltonian of the Wigner crystal with a gapless plasmon mode decoupled from the gapped Ising fermions[6].

5.4. Experimentally observable consequences

As mentioned earlier the computation of observables such as the conductance is complicated due to the importance of the coupling to leads. One may speculate, however, how the above findings affect observables.

The experimentally most relevant observable is the conductance. For noninteracting electrons, the second subband opens a new channel in the wire and, therefore, at the transition

[6] A more careful treatment [75] shows that at strong interactions the weak coupling of the two modes is marginally irrelevant and leads to relatively insignificant corrections to the Ising picture of the transition.

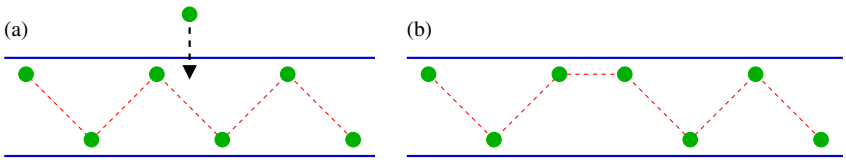

Figure 15. (a) Tunneling into a zigzag crystal. (b) In addition to exciting the plasmon mode, the tunneling electron creates a defect. The finite energy cost associated with the process manifests itself in a gap in the tunneling density of states.

the conductance doubles from $G = e^2/h$ to $G = 2e^2/h$ (for spinless electrons). In the interacting case, however, the second mode is gapped. One might argue [76] that the total charge mode (plasmon) remains gapless and, therefore, one should still expect a doubling of the conductance at the transition. However, as discussed in section 2, the conductance is not determined by the total charge mode only. As the wire is coupled to leads, mixing between different channels occurs and, therefore, modes other than the total charge mode do affect the conductance. We expect that in this case, too, the fact that the second mode is gapped leads to a suppression of the conductance which should remain at its one-dimensional value of $G = e^2/h$ until the second mode becomes gapless at a higher density. This means that the transition from a one-dimensional state to a quasi-one-dimensional state and the step in conductance no longer coincide. Only at higher temperatures $T > \Delta$ does the gapped mode open for transport. Thus, the presence of a gapped mode is expected to lead to non-trivial temperature dependence of the conductance.

The gapped mode above the transition should manifest itself most clearly in the tunneling density of states. Consider the Wigner crystal limit. In the one-dimensional case, the addition of an electron to the system requires the excitation of the plasmon mode in order to adjust the density along the wire. Due to the stiffness of the plasmon mode, the tunneling density of states is suppressed: as discussed in section 2.1 the Wigner crystal described as an elastic medium can be viewed as a Luttinger liquid, and the tunneling density of states of a Luttinger liquid is well known to display a power-law suppression at the Fermi level [77, 78]. In the zigzag crystal, the addition of an electron to the system also requires to adjust the density along the wire by exciting plasmons which suggests a power-law suppression of the density of states. Apart from that, however, the addition of an electron creates a defect in the zigzag structure: the electron is added to one of the two rows and, thus, interrupts the zigzag pattern as depicted in figure 15. The energy of such a defect is finite, and, therefore, the density of states acquires a gap.

This behavior is not limited to the Wigner crystal. As discussed in [76], at any interaction strength tunneling of a single electron into the bulk of the wire excites both the gapless and the gapped mode[7], and the finite energy cost associated with excitation of the gapped mode entails a gap in the tunneling density of states. Consequently the observation of a gap opening in the tunneling density of states would allow one to identify the transition to the quasi-one-dimensional state.

[7] Within the formulation presented here, this can be understood by going back to the unitary transformation (56) which relates the original degrees of freedom described by Hamiltonian (55) to the new degrees of freedom described by Hamiltonian (57). In particular, applying the unitary transformation to the single electron creation operators $\psi_j^\dagger$, where $j = 1, 2$ is the subband index, one may verify that $\psi_1^\dagger$ as well as $\psi_2^\dagger$ contain contributions from both the gapless and the gapped mode of (57).

6. Conclusion

The Luttinger liquid physics of one-dimensional electron systems with weak to moderate interactions has been studied extensively. The present review focuses on novel phenomena due to *strong* interactions which lead to the formation of a Wigner crystal [27]. The strongly interacting regime can be realized experimentally, and evidence for Wigner crystal physics has been seen in the conductance of quantum wires [79, 80], the Coulomb blockade peaks in carbon nanotubes [81], and possibly [82, 83] in the localization features in double quantum wires [84, 85]. While no phase transition takes place, at stronger interactions the system properties change due to the presence of two very different energy scales, namely the Fermi energy E_F and the spin exchange energy $J \ll E_F$. In the strictly one-dimensional regime, one of the main features of Luttinger liquid physics is spin–charge separation [7]. In an inhomogeneous Wigner crystal wire, however, spin physics is found to affect the conductance, reducing it from $2e^2/h$ at $T \ll J$ to e^2/h in the temperature regime $J \ll T \ll E_F$ as discussed in section 2.

Real systems are never strictly one-dimensional, but confined by an external potential. The presence of transverse degrees of freedom leads to a transition from a one-dimensional to a zigzag Wigner crystal at a finite electron density, see section 3. In contrast to the one-dimensional crystal, the zigzag Wigner crystal displays a variety of spin ground states as a function of density, see section 4. In particular, a ferromagnetic ground state—which has been suggested as a possible cause of the conductance anomalies observed in quantum wires [12]—can be realized. While for noninteracting electrons the transition to a quasi-one-dimensional state entails the emergence of a second gapless excitation mode, this is not the case in the presence of interactions. As discussed in section 5, the orbital degrees of freedom are strongly affected by interactions which, for example, are expected to lead to a gap in the tunneling density of states. The most interesting properties of the quasi-one-dimensional state in quantum wires are summarized in the phase diagrams figure 8 (spin properties) and figure 14 (orbital properties).

Figure 8 shows the spin phases of the zigzag Wigner crystal obtained under the assumption that spin and orbital

properties can be treated separately. This approach is justified at strong interactions, when the energy scales for spin and charge excitations are very different, $J \ll E_F$. However, as interactions become weaker the crystal starts to melt, leading to the coupling of spin and orbital degrees of freedom. To study the behavior of the system in this regime, one needs to develop a theory that treats spin and orbital degrees of freedom on equal footing. This entails a number of open questions: are there remnants of the Wigner crystal phase dominated by the four-particle ring exchange in the weakly interacting quasi-one-dimensional state? Is the spectral gap discussed in section 5 robust to the inclusion of spin?

Figure 14 summarizes the orbital properties of the electron system in a quantum wire near the transition from a one-dimensional to a quasi-one-dimensional state. The upper line indicates the vanishing of the gap in the second excitation mode. While the appearance of a second gapless excitation at a finite distance above the transition has been shown in the limit of weak interactions [65], more careful treatment is required to explore this phenomenon at finite interaction strength. In the opposite limit of strong interactions, with increasing electron density the zigzag regime eventually breaks down, giving way to structures with more than two rows. Numerical study of the quasi-one-dimensional Wigner crystal [32] shows that the number of rows changes as $2 \to 4 \to 3 \to 4 \to 5 \cdots$ as a function of density. Since in a wide channel the electron density is not uniform across the wire [86, 87], this trend cannot persist up to an arbitrarily high number of rows. Instead one expects that structures with defects will have a lower energy. The presence of such potentially mobile defects will be crucial for understanding transport properties of quantum wires in that regime.

Acknowledgments

This work was supported by the US Department of Energy, Office of Science, under Contract Nos DE-AC02-06CH11357 and DE-FG02-07ER46424. We acknowledge our collaborators on various projects included in this review: Akira Furusaki, Leonid Glazman, Toshiya Hikihara, Alexios Klironomos, Anatoly Larkin, and Revaz Ramazashvili. Furthermore, we thank the Aspen Center for Physics, where part of this review was written, for hospitality.

References

[1] van Wees B J, van Houten H, Beenakker C W J, Williamson J G, Kouwenhoven L P, van der Marel D and Foxon C T 1988 *Phys. Rev. Lett.* **60** 848
[2] Wharam D A, Thornton T J, Newbury R, Pepper M, Ahmed H, Frost J E F, Hasko D G, Peacock D C, Ritchie D A and Jones G A C 1988 *J. Phys. C: Solid State Phys.* **21** L209
[3] Tarucha S, Honda T and Saku T 1995 *Solid State Commun.* **94** 413
[4] Yacoby A, Stormer H L, Wingreen N S, Pfeiffer L N, Baldwin K W and West K W 1996 *Phys. Rev. Lett.* **77** 4612
[5] Tans S J, Devoret M H, Dai H, Thess A, Smalley R E, Geerligs L J and Dekker C 1997 *Nature* **386** 474
[6] Bockrath M, Cobden D H, McEuen P L, Chopra N G, Zettl A, Thess A and Smalley R E 1997 *Science* **275** 1922
[7] Giamarchi T 2004 *Quantum Physics in One Dimension* (Oxford: Clarendon)
[8] Landauer R 1970 *Phil. Mag.* **21** 863
[9] Maslov D L and Stone M 1995 *Phys. Rev.* B **52** R5539
[10] Ponomarenko V V 1995 *Phys. Rev.* B **52** R8666
[11] Safi I and Schulz H J 1995 *Phys. Rev.* B **52** R17040
[12] Thomas K J, Nicholls J T, Simmons M Y, Pepper M, Mace D R and Ritchie D A 1996 *Phys. Rev. Lett.* **77** 135
[13] Thomas K J, Nicholls J T, Appleyard N J, Simmons M Y, Pepper M, Mace D R, Tribe W R and Ritchie D A 1998 *Phys. Rev.* B **58** 4846
[14] Thomas K J, Nicholls J T, Pepper M, Tribe W R, Simmons M Y and Ritchie D A 2000 *Phys. Rev.* B **61** R13365
[15] Crook R, Prance J, Thomas K J, Chorley S J, Farrer I, Ritchie D A, Pepper M and Smith C G 2006 *Science* **312** 1359
[16] Kristensen A, Bruus H, Hansen A E, Jensen J B, Lindelof P E, Marckmann C J, Nygård J, Sørensen C B, Beuscher F, Forchel A and Michel M 2000 *Phys. Rev.* B **62** 10950
[17] Kane B E, Facer G R, Dzurak A S, Lumpkin N E, Clark R G, Pfeiffer L N and West K W 1998 *Appl. Phys. Lett.* **72** 3506
[18] Reilly D J, Facer G R, Dzurak A S, Kane B E, Clark R G, Stiles P J, Clark R G, Hamilton A R, O'Brien J L, Lumpkin N E, Pfeiffer L N and West K W 2001 *Phys. Rev.* B **63** 121311(R)
[19] Cronenwett S M, Lynch H J, Goldhaber-Gordon D, Kouwenhoven L P, Marcus C M, Hirose K, Wingreen N S and Umansky V 2002 *Phys. Rev. Lett.* **88** 226805
[20] Rokhinson L P, Pfeiffer L N and West K W 2006 *Phys. Rev. Lett.* **96** 156602
[21] Wang C-K and Berggren K-F 1996 *Phys. Rev.* B **54** R14257
[22] Wang C-K and Berggren K-F 1998 *Phys. Rev.* B **57** 4552
[23] Starikov A A, Yakimenko I I and Berggren K-F 2003 *Phys. Rev.* B **67** 235319
[24] Spivak B and Zhou F 2000 *Phys. Rev.* B **61** 16730
[25] Reilly D J, Buehler T M, O'Brien J L, Hamilton A R, Dzurak A S, Clark R G, Kane B E, Pfeiffer L N and West K W 2002 *Phys. Rev. Lett.* **89** 246801
[26] Lieb E and Mattis D 1962 *Phys. Rev.* **125** 164
[27] Wigner E 1934 *Phys. Rev.* **46** 1002
[28] Schulz H J 1993 *Phys. Rev. Lett.* **71** 1864
[29] Fiete G A 2007 *Rev. Mod. Phys.* **79** 801
[30] Chaplik A V 1980 *Pis. Zh. Eksp. Teor. Fiz.* **31** 275
Chaplik A V 1980 *JETP Lett.* **31** 252 (Engl. Transl.)
[31] Hasse R W and Schiffer J P 1990 *Ann. Phys.* **203** 419
[32] Piacente G, Schweigert I V, Betouras J J and Peeters F M 2004 *Phys. Rev.* B **69** 045324
[33] Glazman L I, Ruzin I M and Shklovskii B I 1992 *Phys. Rev.* B **45** 8454
[34] Häusler W 1996 *Z. Phys.* B **99** 551
[35] Matveev K A 2004 *Phys. Rev. Lett.* **92** 106801
[36] Matveev K A 2004 *Phys. Rev.* B **70** 245319
[37] Matveev K A, Furusaki A and Glazman L I 2007 *Phys. Rev. Lett.* **98** 096403
[38] Matveev K A, Furusaki A and Glazman L I 2007 *Phys. Rev.* B **76** 155440
[39] Faddeev L D and Takhtajan L A 1981 *Phys. Lett.* A **85** 375
[40] Haldane F D M 1982 *Phys. Rev.* B **25** R4925
[41] Okamoto K and Nomura K 1992 *Phys. Lett.* A **169** 433
[42] Eggert S 1996 *Phys. Rev.* B **54** R9612
[43] Majumdar C K and Ghosh D K 1969 *J. Math. Phys.* **10** 1388
[44] Majumdar C K and Ghosh D K 1969 *J. Math. Phys.* **10** 1399
[45] Thouless D J 1965 *Proc. Phys. Soc. Lond.* **86** 893
[46] Roger M 1984 *Phys. Rev.* B **30** 6432
[47] Katano M and Hirashima D S 2000 *Phys. Rev.* B **62** 2573
[48] Voelker K and Chakravarty S 2001 *Phys. Rev.* B **64** 235125
[49] Bernu B, Candido L and Ceperley D M 2001 *Phys. Rev. Lett.* **86** 870

[50] Klironomos A D, Ramazashvili R R and Matveev K A 2005 *Phys. Rev.* B **72** 195343
[51] Fogler M M and Pivovarov E 2005 *Phys. Rev.* B **72** 195344
[52] Fogler M M and Pivovarov E 2006 *J. Phys.: Condens. Matter* **18** L7
[53] Klironomos A D, Meyer J S and Matveev K A 2006 *Europhys. Lett.* **74** 679
[54] Klironomos A D 2006 unpublished
[55] Klironomos A D, Meyer J S, Hikihara T and Matveev K A 2007 *Phys. Rev.* B **76** 075302
[56] White S R and Affleck I 1996 *Phys. Rev.* B **54** 9862
[57] Hamada T, Kane J, Nakagawa S and Natsume Y 1988 *J. Phys. Soc. Japan* **57** 1891
[58] Tonegawa T and Harada I 1989 *J. Phys. Soc. Japan* **58** 2902
[59] Chubukov A V 1991 *Phys. Rev.* B **44** 4693
[60] Allen D, Essler F H L and Nersesyan A A 2000 *Phys. Rev.* B **61** 8871
[61] Itoi C and Qin S 2001 *Phys. Rev.* B **63** 224423
[62] Danneau R, Clarke W R, Klochan O, Micolich A P, Hamilton A R, Simmons M Y, Pepper M and Ritchie D A 2006 *Appl. Phys. Lett.* **88** 012107
[63] Klochan O, Clarke W R, Danneau R, Micolich A P, Ho L H, Hamilton A R, Muraki K and Hirayama Y 2006 *Appl. Phys. Lett.* **89** 92105
[64] Danneau R, Klochan O, Clarke W R, Ho L H, Micolich A P, Simmons M Y, Hamilton A R, Pepper M and Ritchie D A 2008 *Phys. Rev. Lett.* **100** 016403
[65] Meyer J S, Matveev K A and Larkin A I 2007 *Phys. Rev. Lett.* **98** 126404
[66] Meyer J S and Matveev K A 2007 unpublished
[67] Reyes S A and Tsvelik A M 2006 *Phys. Rev.* B **73** 220405(R)
[68] Mattis D C 1965 *Theory of Magnetism* (New York: Harper and Row) chapter 9
[69] Vaks G A and Larkin A I 1965 *Zh. Eksp. Teor. Fiz.* **49** 975
Vaks G A and Larkin A I 1966 *Sov. Phys.—JETP* **22** 678 (Engl. Transl.)
[70] See e.g. , Polyakov A M 1987 *Gauge Fields and Strings* (New York: Harwood Academic)
[71] Muttalib K A and Emery V J 1986 *Phys. Rev. Lett.* **57** 1370
[72] Fabrizio M 1993 *Phys. Rev.* B **48** 15838
[73] Ledermann U and Le Hur K 2000 *Phys. Rev.* B **61** 2497
[74] Balents L 2000 *Phys. Rev.* B **61** 4429
[75] Sitte M, Rosch A, Meyer J S, Matveev K A and Garst M 2008 in preparation
[76] Starykh O A, Maslov D L, Häusler W and Glazman L I 2000 *Interactions and Quantum Transport Properties of Lower Dimensional Systems* (*Springer Lecture Notes in Physics* vol 544) ed T Brandes (New York: Springer) p 37
[77] Dzyaloshinskii I E and Larkin A I 1973 *Zh. Eksp. Teor. Fiz.* **65** 411
Dzyaloshinskii I E and Larkin A I 1974 *Sov. Phys.—JETP* **38** 202 (Engl. Transl.)
[78] Luther A and Peschel I 1974 *Phys. Rev.* B **9** 2911
[79] Hew W K, Thomas K J, Farrer I, Anderson D, Ritchie D A and Pepper M 2008 *Physica* E **40** 1645
[80] Hew W K, Thomas K J, Pepper M, Farrer I, Anderson D, Jones G A C and Ritchie D A 2008 *Phys. Rev. Lett.* **101** 036801
[81] Deshpande V V and Bockrath M 2008 *Nat. Phys.* **4** 314
[82] Shulenburger L, Casula M, Senatore G and Martin R M 2008 *Phys. Rev.* B **78** 165303
[83] Guclu A D, Umrigar C J, Jiang H and Baranger H U 2008 arXiv:0807.4292
[84] Auslaender O M, Yacoby A, de Picciotto R, Baldwin K W, Pfeiffer L N and West K W 2002 *Science* **295** 825
[85] Auslaender O M, Steinberg H, Yacoby A, Tserkovnyak Y, Halperin B I, Baldwin K W, Pfeiffer L N and West K W *Science* **308** 88
[86] Larkin I A and Shikin V B 1990 *Phys. Lett.* A **151** 335
[87] Chklovskii D B, Matveev K A and Shklovskii B I 1993 *Phys. Rev.* B **47** 12605